COMPARATIVE STUDY OF NAPHTHALOCYANINE-BASED NEAR-INFRARED ORGANIC PHOTODIODE USING VTTBNc:$PC_{61}BM$ AND VTTBNc:$PC_{71}BM$ BLEND FILMS

SITI ANIS KHAIRANI BINTI ALWI

FACULTY OF SCIENCE

UNIVERSITI MALAYA

KUALA LUMPUR

2022

COMPARATIVE STUDY OF NAPHTHALOCYANINE-BASED NEAR-INFRARED ORGANIC PHOTODIODE USING VTTBNc:$PC_{61}BM$ AND VTTBNc:$PC_{71}BM$ BLEND FILMS

SITI ANIS KHAIRANI BINTI ALWI

DISSERTATION SUBMITTED IN FULFILLMENT OF THE REQUIREMENTS FOR THE DEGREE OF MASTER OF SCIENCE

DEPARTMENT OF PHYSICS

FACULTY OF SCIENCE

UNIVERSITI MALAYA

KUALA LUMPUR

2022

UNIVERSITI MALAYA

ORIGINAL LITERARY WORK DECLARATION

Name of Candidate: **SITI ANIS KHAIRANI BINTI ALWI**

Matric No: **17158405/2**

Name of Degree: **MASTER OF SCIENCE**

Title of Dissertation ("this Work"):

COMPARATIVE STUDY OF NAPHTHALOCYANINE-BASED NEAR-INFRARED ORGANIC PHOTODIODE USING VTTBNc:$PC_{61}BM$ AND VTTBNc:$PC_{71}BM$ BLEND FILMS

Field of Study: **EXPERIMENTAL PHYSICS**

I do solemnly and sincerely declare that:

(1) I am the sole author/writer of this Work;
(2) This Work is original;
(3) Any use of any work in which copyright exists was done by way of fair dealing and for permitted purposes and any excerpt or extract from, or reference to or reproduction of any copyright work has been disclosed expressly and sufficiently and the title of the Work and its authorship have been acknowledged in this Work;
(4) I do not have any actual knowledge nor do I ought reasonably to know that the making of this work constitutes an infringement of any copyright work;
(5) I hereby assign all and every rights in the copyright to this Work to the University of Malaya ("UM"), who henceforth shall be owner of the copyright in this Work and that any reproduction or use in any form or by any means whatsoever is prohibited without the written consent of UM having been first had and obtained;
(6) I am fully aware that if in the course of making this Work I have infringed any copyright whether intentionally or otherwise, I may be subject to legal action or any other action as may be determined by UM.

Candidate's Signature Date: **1/4/2022**

Subscribed and solemnly declared before,

Witness's Signature Date: **1/4/2022**

Name:

Designation:

COMPARATIVE STUDY OF NAPHTHALOCYANINE-BASED NEAR-INFRARED ORGANIC PHOTODIODE USING VTTBNc:$PC_{61}BM$ AND VTTBNc:$PC_{71}BM$ BLEND FILMS

ABSTRACT

In this work, the experimental evaluation of solution-processed bulk heterojunction organic photodiodes using vanadyl 2,11,20,29-tetra-tert-butyl-2,3-naphthalocyanine (VTTBNc) as an electron donor has been presented. VTTBNc is blended with two different fullerene derivatives and served as electron acceptor in which influence the performance of organic photodiode (OPD). The fullerene derivatives involved are [6,6]phenyl-C61-butyric acid methyl ester ($PC_{61}BM$) and [6,6]phenyl-C71-butyric acid methyl ester ($PC_{71}BM$). Three different ratios (1:0.5, 1:1.0, 1:1.5) (vol:vol) of VTTBNc:$PC_{61}BM$ and VTTBNc:$PC_{71}BM$ blend films have been varied in the characterization and optimization of the OPD devices. The blended film of the ratio 1:1.5 and 1:1.0 were found to be the optimized based on the OPD performance for VTTBNc:$PC_{61}BM$ and VTTBNc:$PC_{71}BM$, respectively. The blend film of VTTBNc:$PC_{71}BM$ (vol:vol 1:1.0) exhibits the highest performance in the VTTBNc blend structure with 2.31×10^9 Jones detectivity and 26.11 mA/W responsivity at -1 V bias. Besides that, the blend by using $PC_{71}BM$ shows the enhancement of the morphology as it exhibits higher visibility of the cluster on the surface with surface roughness increased to 62%. The light absorption measurement demonstrated that VTTBNc in the blend film can extend the absorption to the near-infrared (NIR) region furthering in more application for the photodiode. Moreover, the HOMO-LUMO levels of VTTBNc were found to be as -5.14 eV and -3.74 eV which properly aligned with the energy levels in fullerene derivatives.

Keywords: Organic Photodiode, VTTBNc, Fullerene, solution-processed, bulk-heterojunction.

KAJIAN PERBANDINGAN FOTODIOD ORGANIK BERHAMPIRAN-INFRAMERAH YANG BERASASKAN NAPHTHALOCYANINE DENGAN MENGGUNAKAN FILEM CAMPURAN VTTBNc:PC_{61}BM DAN VTTBNc:PC_{71}BM

ABSTRAK

Dalam kajian ini, penilaian eksperimen bagi larutan diproses fotodiod organik heterosimpang pukal menggunakan vanadyl 2,11,20,29-tetra-tert-butyl-2,3-naphthalocyanine (VTTBNc) sebagai penderma elektron telah dibentangkan. VTTBNc diadunkan dengan dua terbitan fulerena yang berbeza yang bertindak sebagai penerima elektron yang memberi pengaruh kepada prestasi fotodiod organik (OPD). Terbitan fulerena yang terlibat adalah [6,6]phenyl-C61-butyric acid methyl ester (PC_{61}BM) dan [6,6]phenyl-C71-butyric acid methyl ester (PC_{71}BM). Tiga nisbah berbeza (1:0.5, 1:1.0, 1:1.5) untuk VTTBNc:PC_{61}BM dan VTTBNc:PC_{71}BM filem telah dimanipulasikan dalam pencirian dan pengoptimuman peranti OPD. Filem campuran nisbah 1:1.5 dan 1:1.0 didapati sebagai nisbah optimum untuk VTTBNc:PC_{61}BM dan VTTBNc:PC_{71}BM. Filem campuran VTTBNc:PC_{71}BM dengan nisbah volumetrik 1:1.0 menunjukkan prestasi tertinggi dalam struktur campuran VTTBNc dengan pengesanan 2.31×10^9 Jones dan responsiviti 26.11 mA/W pada pincangan -1 V. Selain itu, campuran menggunakan PC_{71}BM menunjukkan peningkatan morfologi kerana ia memperlihatkan kumpulan tompok yang lebih tinggi pada permukaan dengan kekasaran permukaan meningkat ke 62%. Pengukuran penyerapan cahaya yang ditunjukkan VTTBNc dalam filem campuran menunjukkan penyerapan pada kawasan inframerah hampir (NIR) dan membuka lebih banyak peluang untuk digunakan sebagai aplikasi untuk fotodiod. Tambahan pula, tahap HOMO-LUMO VTTBNc didapati sebagai -5.14 eV dan -3.74 eV yang sejajar dengan tahap tenaga fulerena terbitan.

Kata kunci: Fotodiod organik, VTTBNc, Fulerena, proses larutan, heterosimpang pukal.

ACKNOWLEDGEMENT

First and foremost, I am grateful to Allah for granting me the strength and determination in completing this work. As a Muslim, “Alhamdulillah” is the perfect word for me to address my gratitude. Besides, I am thankful to my beloved parents, Alwi bin Omar and Rospaidah binti Endut for their endless moral support and encouragement in educating me to be better. I am also grateful for the financial support given by my parents.

A big thanks to my supervisors, Associate Professor Dr. Azzuliani Supangat and Professor Dr. Siti Rohana Majid for giving me the opportunity to venture into research. The constant guidance from them assisted me to finish the uphill task that I faced. I also appreciate their cooperation and concern that they have shown during the entire course of my study.

I am extending my appreciation and thanks to my group mates, Syaza Nafisah, Afiq Anuar, Atiqah Husna, Ain, Yash, Hanan and Dr. Azmina for their support since the first day I joined the group. Additionally, I am very thankful to Dr. Shahino Mah for his guidance and support through my study. I am also thankful to the Low Dimensional Materials Research Centre (LDMRC) staff, Dr. Arif Sarjidan and Mrs. Aida Hani, for their assistance that facilitated my work in the laboratory.

Finally, I would like to acknowledge the Universiti Malaya for providing a financial scheme through the research grant RP039B-18AFR and GPF037B-2018 for the research project funding.

TABLE OF CONTENTS

LIST OF FIGURES

LIST OF TABLES

LIST OF SYMBOLS AND ABBREVIATIONS

D^*	:	Detectivity
e	:	Charge of electron
eV	:	Electron volt
E_{OX}	:	Onset oxidation potential
E_{RED}	:	Onset reduction potential
h	:	Planck's constant
I_{ph}	:	Photocurrent
J_D	:	Dark current density
J_{ph}	:	Photocurrent density
J_{sc}	:	Short-circuit current density
hv	:	Photon energy
q	:	Elementary charge
v	:	Vibrational frequency
V_{oc}	:	Open-circuit voltage
λ	:	Wavelength
AFM	:	Atomic Force Microscopy
Ag	:	Silver
AgCl	:	Silver chloride
Al	:	Aluminium
BHJ	:	Bulk heterojunction
C_{60}	:	Buckminsterfullerene
CE	:	Counter electrode
ClAlPc	:	Chloroaluminium phthalocyanine
CV	:	Cyclic Voltammetry

DI	:	Deionized
EQE	:	External Quantum Efficiency
GeNc	:	Germanium naphthalocyanine
HCl	:	Hydrochloric acid
HOMO	:	Highest Occupied Molecular Orbital
IPCE	:	Incident Photon-to-Current Efficiency
ITO	:	Indium Tin Oxide
J-V	:	Current density – Voltage
LUMO	:	Lowest Unoccupied Molecular Orbital
MEH-PPV	:	Poly[2-methoxy-5-(2'-ethylhexyloxy)-1,4-phenylene vinylene]
MISIM	:	Metal/Insulator/Semiconductor/Insulator/Metal
MISM	:	Metal/Insulator/Semiconductor/ Metal
OPD	:	Organic Photodiode
OPV	:	Organic Photovoltaic
$OSnNcCl_2$	:	Octabutoxy tin naphthalocyanine dichloride
$PC_{61}BM$	:	[6,6]phenyl-C61-butyric acid methyl ester
$PC_{71}BM$	:	[6,6]phenyl-C71-butyric acid methyl ester
PEDOT:PSS	:	poly(3,4-ethylenedioxythiophene) polystyrene sulfonate
PL	:	Photoluminescence
PTCDA	:	Perylenetetracarboxylic dianhydride
PVD	:	Physical Vapour Deposition
RE	:	Reference electrode
R	:	Responsivity
RMS	:	Root mean square
SHE	:	Standard hydrogen electrode
SiNc	:	Silicon naphthalocyanine

SMU	:	Source Measure Unit
$SnNcCl_2$	:	Tin (IV) naphthalocyanine dichloride
SnNPc	:	Sn(II)-2,3-naphthalocyanine
SubPc	:	Subphthalocyanine
UPS	:	Ultraviolet Photoelectron Spectroscopy
UV	:	Ultraviolet
UV-Vis	:	Ultraviolet-visible
VTTBNc	:	Vanadyl 2,11,20,29-tetra-tert-butyl-2,3-naphthalocyanine
VTP	:	Vanadyl 3,10,17,24-tetra-*tert*-butyl-1,8,15,22-tetrakis(dimethylamino)-29*H*,31*H*-phthalocyanine
WE	:	Working Electrode

CHAPTER 1: INTRODUCTION

1.0 Research Background

In recent years, the development of organic materials is growing tremendously for the replacement of inorganic materials in various applications due to their advantages. Photodiodes based on organic materials can be realized in broad-band spectrum wavelength or it can be tuned to specific wavelength corresponding to the application of the photodiode. Unlike inorganic materials, photodiodes based organic materials are lightweight materials denoted by organic polymers, oligomers and small molecules. The fabrication in low temperature over large areas and mechanically flexible on the transparent substrate made organic materials to be a potential as an innovative target among researchers.

Historically, the evolution of organic photodiode (OPD) is in line with the evolution of organic photovoltaic (OPV). It is because both devices share the same working principle which converts light energy into the electrical signal. Moreover, both the invention of OPD and OPV used the same components in fabricating the devices. The invention of organic photodiodes was started since 1981 by Kudo and Moriizumi that covered spectral response in the visible range (Kudo & Moriizumi, 1981). Merocyanine and rhodamine B have been used as photoactive layers that were deposited by a sublimation method in vacuum. The structure employed in this experiment was fabricated in the inverted structure. Later in 1986, a photovoltaic cell utilizing organic small molecules with power conversion of about 1% was reported (Tang, 1986). The small molecules used in this study are copper phthalocyanine and perylene tetracarboxylic derivatives which are deposited in bilayer structure through vacuum evaporation method. The performance of the OPV devices in this study was investigated by measuring current-voltage characteristics under AM2 illumination (75 mW/cm^2).

In 1992, the suppression of photoluminescence is observed to demonstrate the photoinduced electron transfer of conjugated polymer and fullerene (Morita, Zakhidov, & Yoshino, 1992; Niyazi S Sariciftci, Smilowitz, Heeger, & Wudl, 1992). The electron transfer between these two materials implies the role of donor and acceptor phase separation. A year later in 1993, Sariciftci et al. utilized conjugated polymer and fullerene in the study of photovoltaic and photodiode performance (Niyazi Serdar Sariciftci et al., 1993). The device structure is composed of MEH-PPV and buckminsterfullerene, C_{60} as the photoactive layer which has been fabricated in bilayer structure through spin coating method. The study achieved power conversion efficiency of 0.04% and the ON/OFF current ratio of $6x10^3$ at -1V bias. In 1994, Yu et al. introduced the first solution-processed bulk heterojunction photodiode based on polymer-fullerene blend (G Yu, Pakbaz, & Heeger, 1994). The bulk heterojunction structure composed of MEH-PPV and C_{60} blend in a 10:1 wt. % ratio with photosensitivity of 5.5 mA/W at zero bias. However, Yu et al. faced a difficulty in the film formation as high concentration of C_{60} used in the blends. This is due to C_{60} having limited solubility in organic solvents and tends to crystallize during the film formation. In 1995, Yu et al. discovered the use of soluble C_{60} derivative in enhancing the performance of polymer-fullerene bulk heterojunction (Gang Yu, Gao, Hummelen, Wudl, & Heeger, 1995). This study shows the enhancement in photosensitivity of 100 mA/W with quantum efficiency of 29% has been achieved.

During the rapid development of solution-processed bulk heterojunction, the study of the solution-processable small molecules began to appear. In 2001, Schmidt-Mende et al. introduced the solution-processable small molecule blends, which used self-organized photovoltaic structure (Schmidt-Mende et al., 2001). The structure consists of Perylene and HBC-PhC12 as the photoactive layer and achieved power efficiencies near to 2%. In 2010, solution-processable photovoltaic of phthalocyanine derivative and fullerene was studied. The structure containing $C6PcH_2$:PCBM small molecules deposited by spin

coating method has demonstrated energy conversion efficiency of 3.1% (Hori et al., 2010). Afterwards, the study of solution-processed organic photodiodes based on porphyrin small molecules and fullerene has been carried out in 2014 (Li, Huang, Peng, Cao, & Peng, 2014). The photodiode demonstrated a broad spectral response from 380 to 960 nm with ON/OFF current ratio of about 10^5 at zero bias.

For the detection in the NIR region, the continuous effort in the OPD's development has been made, which drives the utilization of low band gap materials. Thus, the exploration of the small molecules and conjugated polymers with absorption in the longer wavelength has become the main focus in developing NIR OPD. In the case of small molecules, phthalocyanines have been widely used as a donor for the fabrication of NIR OPD. Hence, a recent study on vacuum-processed phthalocyanine-based NIR OPD has achieved detectivity of 10^{13} Jones and responsivity of 0.439 A/W at -2V bias by utilizing ClAlPc and fullerene as the photoactive layer (Lee et al., 2020). Meanwhile, for the solution-processed, there are still limited studies on the phthalocyanine-based NIR OPD. In 2018, Roslan et al. demonstrated solution-processable phthalocyanine NIR OPD using VTP and $PC_{71}BM$ (Roslan, Abdullah, Abd Majid, & Supangat, 2018). This study claims to obtain absorption coverage up to 900 nm with 0.23 A/W of responsivity at -1 V bias. The tuneability of the band gap in semiconducting polymer by chemical design has led to the discovery of the low band gap polymer (Scharber & Sariciftci, 2021). In 2018, Zheng et al. demonstrated low bandgap conjugated copolymer OPD by using PBBTPD:Tri-$PC_{61}BM$ with detectivity up to 10^{11} Jones at -0.5 V in the broadband spectral response from 350 nm to 2500 nm (Zheng et al., 2018). In 2021, Lau et al. fabricated transparent NIR OPD using low band gap polymer (COi8DFIC) with high transparency of 92% (Lau, Lan, Cai, & Zhu, 2021). The study achieved 0.28 A/W of responsivity and 10^{12} Jones of detectivity. Figure 1.1 summarizes the milestone in the development of organic photodiodes.

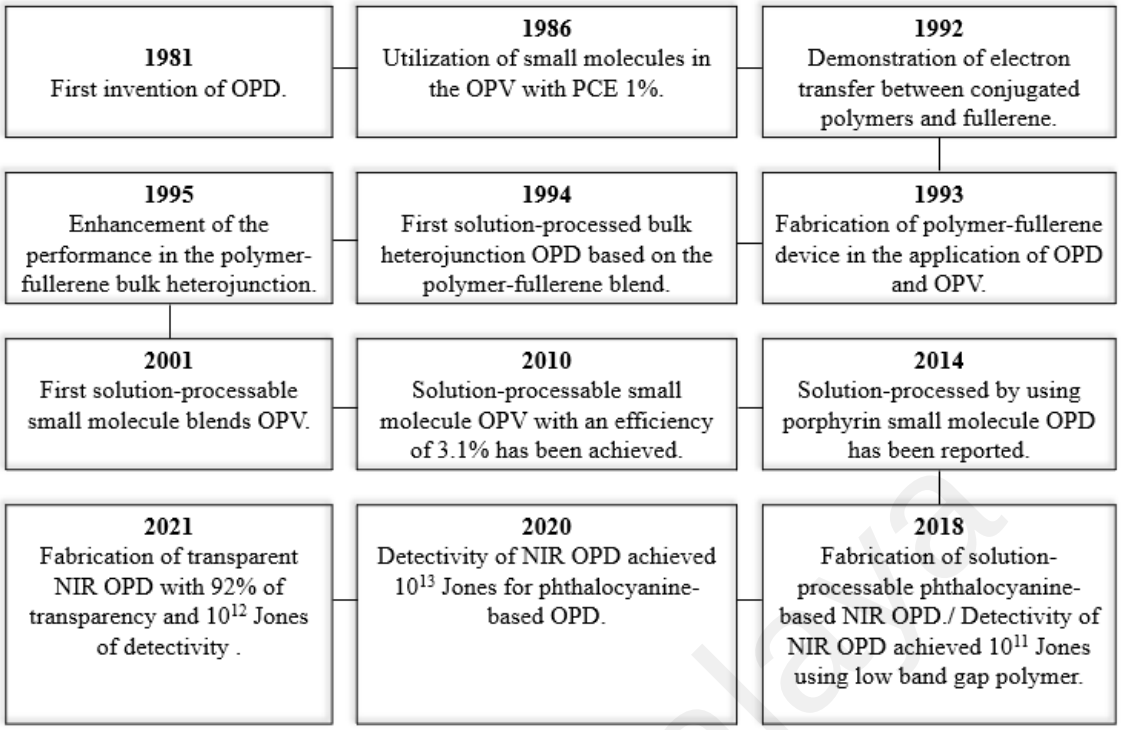

Figure 1.1: Milestone in development of organic photodiodes.

1.1 Problem Statement

Recently, the performance of solution-processed NIR OPD has achieved 10^{12} Jones of detectivity by using low band gap polymer (Lau et al., 2021). While NIR OPD utilizing solution-processable small molecules are still low in performance (Roslan et al., 2018; Zafar, Fatima, Karimov, Ahmed, & Sulaiman, 2017). This is due to the fact that solution-processed based on small molecules OPD is still new in the research area. In small molecules, phthalocyanines are the most well-known small molecules and are widely used in the fabrication of NIR OPD due to their excellent properties, such as high stability and efficient light absorption. For these materials, vacuum deposition is the most favourable method to fabricate phthalocyanine-based OPD. This is due to the fact that most of the phthalocyanines are insoluble or barely soluble in organic solvents (Ghani, Kristen, & Riegler, 2012). Therefore, the synthesize of phthalocyanine by adding substituents in the phthalocyanine has been introduced to increase the solubility in organic solvents (Nemykina & Lukyanets, 2010). Since naphthalocyanine is a derivative of

phthalocyanine, thus the properties of these materials are still the same. Although there are few numbers of studies based on substituted phthalocyanine and naphthalocyanine OPD have been reported, there is no comprehensive study in the evaluation of OPD's performance. Thus, a comprehensive study in solution-processed OPD using phthalocyanine or naphthalocyanine needs to be done in order to meet the future needs in the OPD's development.

1.2 **Objectives**

In this research, the main study is to fabricate the solution processable organic photodiode (OPD) devices by using small molecules blend that incorporate naphthalocyanine (VTTBNc) and fullerene derivatives ($PC_{61}BM$ & $PC_{71}BM$). The utilization of VTTBNc as an electron donor blended with two different electron acceptors of fullerene derivatives in bulk heterojunction is to offer further understanding in the evaluation of the performance in organic photodiode (OPD). Besides, this study is aimed to explore VTTBNc ability as an electron donor in the OPD structure. The detailed investigations in optical, structural, morphological and electrical characterization have been observed to have deep understanding in OPD's performance trend. Therefore, the objectives of this study can be summarized as follows:

i. To achieve broad spectral range of optical absorption between 300 nm and 900 nm.
ii. To determine the energy band gap of naphthalocyanine.
iii. To evaluate the role of difference fullerenes in the dark current density and photocurrent density to the performance of naphthalocyanine:fullerene NIR organic photodiode.

1.3 **Thesis outline**

Chapter 1 initially includes the research background of photodiode. Then, it is followed by the problem statement of the study. The aim and objectives also briefly describe in this chapter where the main study is to evaluate the performance behavior of solution-processable organic photodiode (OPD) devices by using small molecules blend incorporate naphthalocyanine (VTTBNc) and fullerenes derivative ($PC_{61}BM$ & $PC_{71}BM$). Chapter 2 covers the literature reviews which is related to the materials used and the fundamental theory of OPD. The detailed explanation of the device structure and working principle of OPD has been explained. In Chapter 3, the research methodology involved throughout the study has been explained in detail. The methodology includes the process of device fabrication and the characterization used in the experiment. Chapter 4 shows the results obtained and the result analysis. In this study, the evaluation of OPD's analysis result is divided into three parts. The first part consists of the study of the photoactive layer's absorption and the HOMO-LUMO determination of VTTBNc. Then, the performance of OPD devices is evaluated based on the J-V characteristics and EQE graphs. Lastly, further characterization in the characterization of the photoactive layer has been discussed based on the OPD devices performance. The characterization includes optical, structural and morphological.

CHAPTER 2: LITERATURE REVIEW

2.0 Overview

Chapter 2 discussed the organic semiconductors of the materials involved, working principle, device structure and the performance evaluation of OPD. The first part of this chapter begins with the discussion on the organic semiconductors related to the materials involved which includes the previous study on naphthalocyanine-based OPD. Then, a detailed view on the device structure of OPD which includes the main reason for the used bulk-heterojunction has been discussed. Further, the working principle of OPD has been discussed. Lastly, the last part of this chapter discussed the basic information of the performance evaluation of OPD.

2.1 Organic semiconductors

Organic semiconductors are the class of materials derived from sp^2 hybridized carbon atoms. Hybridized orbitals contain up to three strongly localized covalent σ-bonds which represent the molecular backbone, meanwhile the remaining half-filled p-orbitals are known as π-bonds in which delocalization of the molecule occurred (π-conjugation). P-orbitals are the frontier orbitals that are in charge of the optoelectronic properties of a molecule. The frontier orbitals are often taken as the interaction between the highest occupied molecular orbital (HOMO) and the lowest unoccupied molecular orbital (LUMO). Oversimplifying, the concept of HOMO and LUMO levels are fundamentally same with the valence and conduction band in inorganic semiconductor. Organic semiconductors can be referred to as small molecules, oligomers (repetition of few monomer units) and polymers (repetition of many monomer units). Conjugated chains in the molecule generally determine the HOMO and LUMO energy levels and also the bandgap of the polymer (Su, Lan, & Wei, 2012).

2.2 Small molecules materials

Small molecules are an organic compound that possess defined molecular structure with low molecular weight for convenient synthesis and purification. This led to the improvement of the fabrication repeatability as it exhibited a greater tendency to form ordered domains and provide higher charge carrier mobilities (Dong, Zhu, Meng, Gong, & Hu, 2012). These advantages made small molecules as great alternatives to conjugated polymers in bulk heterojunction structure. On top of that, small molecules evade unwanted features of macromolecules like chain twists and chain-end defects that give rise to structural disorder and to low lying trap states (Collins, Ran, Heiber, & Nguyen, 2017). Relatively, small molecules material is inexpensive compared to conjugated polymers. It drives small molecules as reasonable materials to develop compared to the conjugated polymer. Naphthalocyanine and fullerenes are considered as one of the types of the small molecules materials that have been studied.

2.3 Naphthalocyanine derivative (VTTBNc)

Naphthalocyanine is a derivative of phthalocyanine that contains a cross-shaped organic molecule composed of 48 carbons, 8 nitrogen and 26 hydrogen atoms. It has been utilized as pigments and dyes due to the intense blue or green color. The group of this material exhibit attractive properties, such as high thermal and chemical stability, efficient light absorption and contain photo-conducting characteristics (Andzelm, Rawlett, Orlicki, Snyder, & Baldridge, 2007). The stable macrocyclic conjugated network of π-electrons is the root to the properties gained in the naphthalocyanine materials. This led the material to have larger polarizability and sensitivity to the environment of the local electrostatic (Blumenfeld, Steele, Ilyas, & Monti, 2010). The research study based on phthalocyanines and naphthalocyanines have increasing due to the potential ability in the various application (Leem et al., 2021; Ohtani, Nakajima, & Bando, 2011; Roslan et al.,

2018; Zafar et al., 2017). Figure 2.1 shows the molecular structure of vanadyl 2,11,20,29-tetra tert-butyl 2,3 naphthalocyanine (VTTBNc).

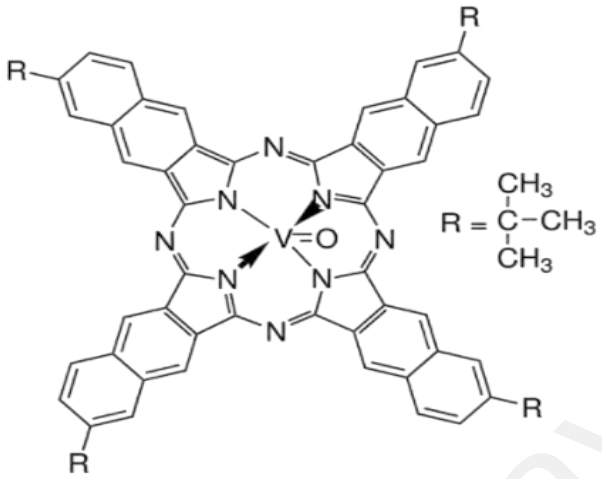

Figure 2.1: The molecular structure of VTTBNc. (Aziz et al., 2018)

2.4 Fullerene ($PC_{61}BM$ and $PC_{71}BM$)

Fullerene is an allotrope of carbon that can form either in a closed cage (etc: buckyball) or in a cylinder (etc: carbon nanotubes). It consists of carbon atoms that are linked by single and double bonds to build a closed or partially closed network. The first breakthrough of fullerene was discovered in the early of 1985 by Kroto et al. (Kroto, Heath, O'Brien, Curl, & Smalley, 1985). Since then, fullerene has been widely used for research development especially in organic photovoltaic and photodiode application.

As we are aware, [6,6]phenyl-C71-butyric acid methyl ester ($PC_{71}BM$) and [6,6]phenyl-C61-butyric acid methyl ester ($PC_{61}BM$) are the most-prominent reported electron acceptor materials. $PC_{71}BM$ and $PC_{61}BM$ are the molecular derivatives of C_{70} and C_{60}, respectively. Figure 2.2 shows the molecular structure of $PC_{61}BM$ and $PC_{71}BM$. Between these two fullerenes, $PC_{61}BM$ is more commonly available as it is an inexpensive material as compared to $PC_{71}BM$ [9]. Besides, $PC_{61}BM$ also has a good carrier mobility, high solubility, low-lying LUMO compared to $PC_{71}BM$. Despite the advantages in $PC_{61}BM$, $PC_{71}BM$ has stronger absorption in the visible region as

compared to $PC_{61}BM$ [10]. It is because $PC_{71}BM$ has lower symmetry and more extended conjugation that lead to a broader photo-absorption profile in the visible region of the electromagnetic spectrum. Therefore, this property has brought $PC_{71}BM$ as most relevant for the application in photodiodes and photovoltaics.

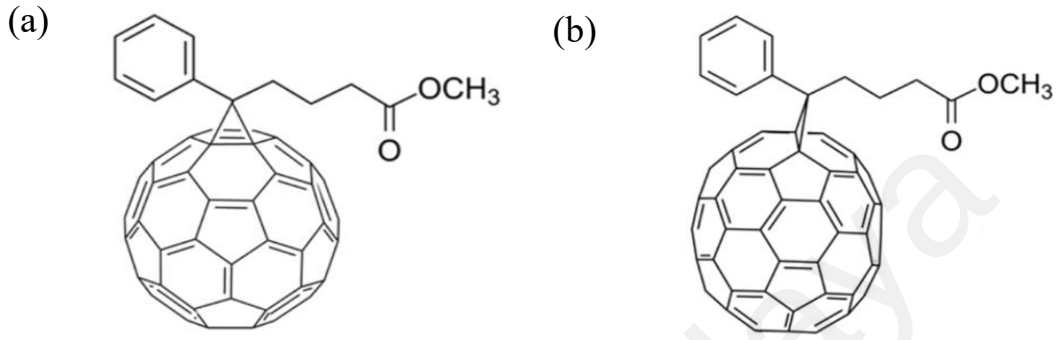

Figure 2.2: Molecular structure of (a) [6,6]phenyl-C61-butyric acid methyl ester ($PC_{61}BM$) and (b) [6,6]phenyl-C71-butyric acid methyl ester ($PC_{71}BM$). (Williams, Tummala, Aziz, Risko, & Brédas, 2014)

2.5 Previous studies on naphthalocyanine-based OPD device

Vacuum deposition is the well-known method in the deposition of naphthalocyanine-based OPD. Most of the OPD fabricated by this method obtained high performance in terms of detectivity and responsivity. Leem et al. manage to acquire $1.85x10^{13}$ Jones of detectivity and 0.32 A/W of responsivity at -1 V bias by compromising $SiNc/C_{60}$ deposited through vacuum deposition process (Leem et al., 2021). In 2018, Reissig et al. demonstrate OPD in which the photoactive layer of Sn(II)-2,3-naphthalocyanine (SnNPc) is sandwiched with two insulating layers or known as MISIM structure (Reissig, Dalgleish, & Awaga, 2018). In this study, the device acquired ~0.12 mA/W of the responsivity at the 850 nm maximum absorption. On top of that, Dalgleish et al. used SnNPc as p-type material with the presence of the ultrathin (1nm) of n-type PTCDA by controlling the crystallinity based on MISM device structure (Dalgleish et al., 2018). The crystallinity was enhanced by increased substrate temperature and achieved ~20 μs of

response time and ~2 mA/W of responsivity. In 2012, Matthew Menke et. al obtained broadband photodetection with responsivity 0.2 A/W by integrating three electron donors (SubPc/ClAlPc/$SnNcCl_2$) deposited through vacuum deposition process (Matthew Menke, Pandey, & Holmes, 2012). Aside from the OPD, organic photovoltaic (OPV) of the naphthalocyanine-based using vacuum deposition method has been introduced (Pandey et al., 2013). The photoactive materials composed of $SnNcCl_2$ and C_{60} are used to obtain optical absorption near to 1100 nm with power conversion efficiency of 1.2%.

Meanwhile, for the solution-processed based on naphthalocyanine OPD deposited through spin-coating method is still limited in the research area. Based on the past study, Campbell developed naphthalocyanine-based ($OSnNcCl_2$) organic photodiode using solution-processed method (Campbell, 2010). In this study, organic photodiodes achieved transparency of ~80% in the visible spectrum and EQE of ~80% at bias near -5V in the NIR region. Then, in 2011, the development of solution-processing of naphthalocyanine material has been achieved by utilizing copper naphthalocyanine as the photoactive layer (Ohtani et al., 2011). In this study, they obtained low dark current which is 5μA by compromising naphthalocyanine material, wide-bandgap polymer and electron acceptor in the OPD structure. Besides OPD, the development of naphthalocyanine-based OPV deposited through solution-processed has been introduced by Yoshida et al. using germanium naphthalocyanine (GeNc) (Yoshida, Oku, Suzuki, Akiyama, & Yamasaki, 2013). The GeNc is added to the OPV structure to extend the light absorption into NIR region and obtained 1% efficiency. Table 2.1 depicts the strength and weakness of previous study on napthalocyanine-based OPD.

Even so, the performance and study of OPD through vacuum deposition process is unbeatable for this type of material. The solution-processed via spin coating method has many characteristics that meet the future needs in the OPD's development. This method can produce a uniform thin film in a short time and low-cost production. Thus, the

exploration of soluble materials in organic solvents is important in the development of OPD performances. From a recent study, VTTBNc is solubilized in organic solvent which is chloroform (Aziz et al., 2018). The exploration of VTTBNc as one of the materials in the OPD structure is needed for the progress of the OPD based on solution processes.

Table 2.1: Strength and weakness of previous study on naphthalocyanine-based OPD.

Methods	References	Strength	Weakness
Vacuum deposition	Leem et al., 2021	Achieved high detectivity.	Using a complex method as it is fabricated in vacuum deposition.
	Reissig et al., 2018	Achieved high bandwidths ~4MHz due to the short response time.	Low in responsivity and the photoactive layer was deposited using vacuum deposition.
	Dalgleish et al., 2018	Achieved fast response time ~20μs.	Low in responsivity and the photoactive layer was deposited using vacuum deposition.
	Matthew Menke et. al., 2012	Achieved broadband response with high efficiency and responsivity.	Using a lot of electron donors and fabricated in vacuum deposition.
Solution-processed	Ohtani et al., 2011	Low dark current (I_D=5μA) obtained.	More materials used for suppressing the dark current.
	Campbell, 2010	Demonstration of transparency ~80%	The insertion of electron transport layer complicates the fabrication of the device. Besides, the responsivity and detectivity values of the devices are not stated.

2.6 Device structure

For the last few years, bulk heterojunctions (BHJ) using solution-processable small molecules as the donor and the acceptor have made their debut as dominant design used in organic photodiodes and solar cells (Hori et al., 2010; Roslan et al., 2018; Schmidt-Mende et al., 2001; Zafar et al., 2017). It has appeared as the most effective idea of organic semiconductors with respect to processing costs. Bulk heterojunction contains a mixture of donor and acceptor as the interpenetrating layer in photodiode devices. In such a structure, the donor acceptor is well distributed in the interpenetrating layer and consequently introducing more charge interface between donor and acceptor within a few nanometres scale. This architecture overcomes the problem encountered in bilayer structure which suffers from limited interfacial area. Figure 2.3 illustrates the device structure of bilayer and bulk heterojunction. This advantage enhances charge separation since the excitons can only move around 5-10 nm from their generation point (Bartelt et al., 2013). Thus, the photoactive layer of the BHJ devices plays a great role in the generation of free carriers and charge transport.

In the BHJ, indium tin oxide (ITO) is a common design to be as the transparent bottom anode and evaporated low work function metals (such as Al) as the top cathode. To ensure a virtually negligible light absorption in the visible range, an additional interlayer of PEDOT: PSS with work function 5.0 eV has usually been added on top of the ITO. It is because ITO (work function 4.7 eV) is not well suited to the hole collection (Natali & Caironi, 2016).

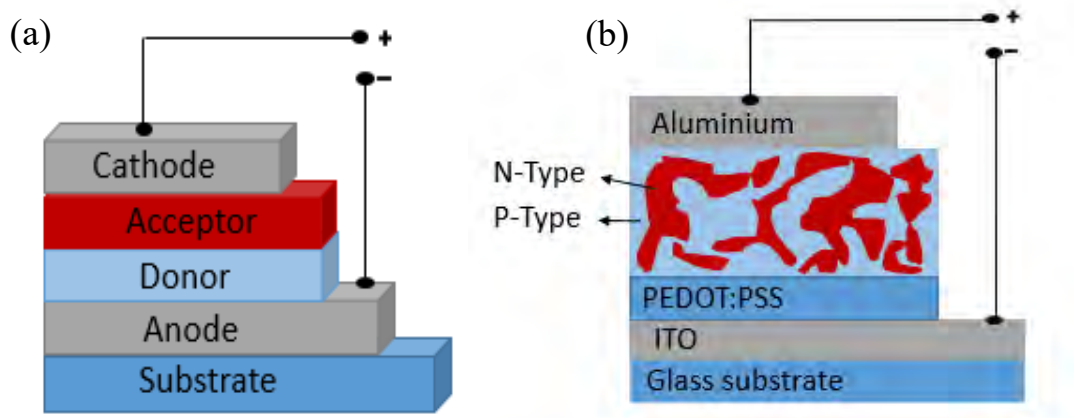

Figure 2.3: The structure of (a) bilayer heterojunction and (b) the bulk heterojunction.

2.7 Working principle in OPD

The working mechanism of photodiodes in organic materials is similar to the inorganic materials which is based on internal photoelectric effect. The internal photoelectric effect refers to the generation of photoelectrons within the materials. The working principle of the organic photodiodes involved four the following steps as illustrated in Figure 2.4:

1. Light absorption
2. Exciton diffusion
3. Charge separation
4. Charge extraction

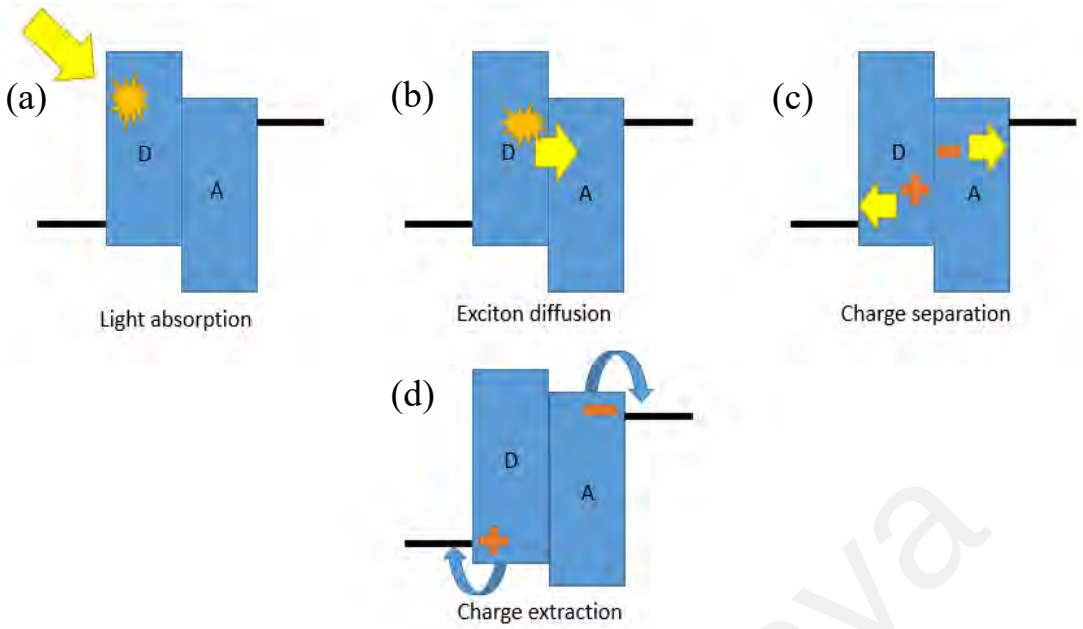

Figure 2.4: The illustrated diagram of the working principle in OPD. (a) Light absorption, (b) Exciton diffusion, (c) Charge separation & (d) Charge extraction.

2.7.1 Light absorption

Light illumination with high enough energy will be absorbed by the photoactive layer in the OPD's device. The energy of the absorbed photons needs to be equal or higher than the band gap of the photoactive layer, in order to excite the electrons from HOMO to LUMO level. In this process, the exciton is generated in the photoactive layer. An exciton is an electron and hole pair that is bound by the electrostatic Coulomb force that attracts an electron and a hole together.

2.7.2 Exciton diffusion

Once the excitons are formed, they diffuse into the interpenetrating layer between donor-acceptor interfaces. The diffusion of exciton is limited to diffusion length around 5-10 nm away from their creation point before it decay back to the HOMO levels. The state where the electron decay back to the original levels is called a recombination process. Therefore, the exciton needs to be diffused in the range of exciton diffusion length to ensure the dissociation of excitons into free electrons and holes pairs. In other

words, the probability of dissociation of excitons is strongly dependent on the number of excitons reaching the donor-acceptor interface.

2.7.3 Charge separation

However, the dissociation of exciton into free electrons and holes does not occur spontaneously without any external force. An electric field has been applied in the organic photodiode in order to assist the dissociation of exciton into free electrons and holes. In this process, the coulomb bound of the exciton will break and cause charge separation. Then, the electron will move to the acceptor and hole will remain at the donor at the interface between donor and acceptor.

2.7.4 Charge extraction

Once the charge separation happened, the separated charge was then collected at the electrode. The external bias applied will help the extraction of electrons and holes travel to its own electrodes. Electrons from the donor will travel to the acceptor and collected at the cathode which is commonly used as an Aluminium. On the other side, holes from the acceptor will travel through the donor and then collected at the anode.

2.8 Performance evaluation of OPD

The current density-voltage (J-V) characteristics and external quantum efficiency (EQE) are the measurements used in the evaluation of the performance of photodiodes. Fundamentally, J-V characteristics provide all the details parameters which include the calculation of responsivity and detectivity values with the influence of dark current values. Meanwhile, EQE demonstrates the photo conversion capability and responsivity in a function of wavelength without the presence in the dark current values. Further role of the measurements has been discussed in the section below.

2.8.1 J-V Characteristics

The Current Density-Voltage (J-V) characteristics in OPD are basically to analyse the overall performance of the device. This characteristic curve shows the relationship between the current flowing through the device and the voltage applied across the terminal. The J-V curve observed in a photodiode is similar to the curve of a normal diode. At the forward bias, there is an exponential increase in the current density while at the reversed biased, there is a small saturation current is measured. Figure 2.5 illustrates the J-V curve observed in a photodiode. There are three operating modes of the photodiode as listed below:

- Photovoltaic mode: In this mode, there is no voltage applied or known as zero-bias mode. In this mode, the photodiode behaves as a solar cell.
- Photoconductive mode: In this mode, the voltage applied is at reversed bias and the measured current is saturated or ideally zero.
- Avalanche diode mode: This mode operates in high reverse bias voltage, which allows the multiplication of avalanche breakdown towards the exciton generated.

In contrast to solar cells, photodiodes are designed to operate in reversed bias which is in a photoconductive mode. In this mode, the photocurrent is linearly proportional to the light illumination received that makes the photodiode ideal for light detection. The reversed bias applied leads to the extremely low current flowing until the electric field is high enough to cause a breakdown. Meanwhile, the solar cell is operated in a photovoltaic mode in which there is no voltage applied. The short circuit current density, J_{sc} and open-circuit voltage, V_{oc} are the basic parameters used for the evaluation of the solar cell performance.

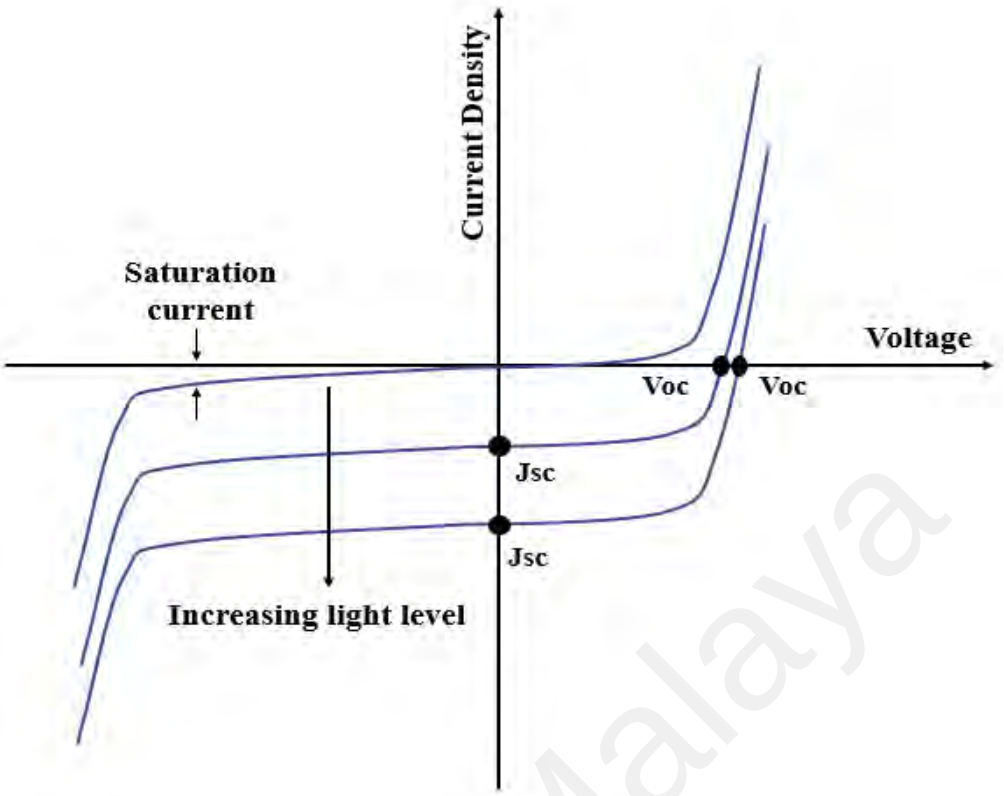

Figure 2.5: The Current Density-Voltage curve of photodiodes in a dark state and with increasing illumination.

In OPD, the essential parameters measured are dark current density and photocurrent density. Photocurrent density is the current generated as the incident light induced in a photodiode. Dark current, or leakage current, is the current that flows through the photodiode in the photoconductive mode with the absence of light. The presence of high dark currents will contribute to the high electronic noise that limits detectivity of OPD. In this case, the noise from thermal noise and flicker noise are assumed to be ignored. The performance evaluation of photodiodes can be calculated from dark current and photocurrent values, in order to determine the responsivity and detectivity values. The responsivity of OPD can be calculated using the following equation:

$$R = \frac{(J_{ph} - J_D)}{P} \tag{2.1}$$

Where R is responsivity, J_{ph} is photocurrent density, J_D is the dark current density and P is power intensity of incident light. Meanwhile, detectivity (D^*) is defined as the ability of OPD to detect a small photon signal. The detectivity, D^* can be express as:

$$D^* = \frac{R}{\sqrt{2q.J_D}} \tag{2.2}$$

Where q is the elementary charge (1.602 x 10^{-19}C). From equation above, the value of $2qJ_D$ is associated with the shot noise caused by dark current.

2.8.2 EQE

External Quantum Efficiency (EQE) is an important parameter that represents the capability of photoelectric conversion of an OPD. For instance, the EQE is the ratio of the number of charge carriers generated by the OPD to the number of the incident light induced. In this measurement, the influence of dark current is excluded as it uses a phase-sensitive detection method. Thus, this measurement allows the OPD to detect a small signal, despite the high noise presented. The EQE can be expressed as:

$$EQE = \frac{I_{ph}/e}{P/hv}\ [\%] \tag{2.3}$$

Where I_{ph} is the measured photocurrent, e is the charge of electrons, P is the power of intensity, h is the Planck's constant and v is the vibrational frequency of the irradiated photon. From this expression, the responsivity can be substituted into the EQE equation to form a new relationship between EQE and responsivity as expressed in the equation below:

$$EQE = \frac{Rx1240}{\lambda}\ x100[\%] \tag{2.4}$$

Where R is responsivity and λ is the wavelength. To be summarized, EQE is one of the most important measurements in analysing the performance of OPD. It involves the measurement of photons being absorbed and the number of charge carriers collected in

the OPD. High EQE indicates a high charge carrier collected from the photon that is induced in the OPD. Thus, a good photoactive layer in the OPD devices has a low charge recombination rate. Charge recombination can cause a reduction of the EQE values.

CHAPTER 3: METHODOLOGY

3.0 Overview

Chapter 3 describes the methodology of the fabrication and characterization of OPD devices. Firstly, this chapter describes the fabrication process involved in this study which includes the substrate's preparation and cleaning, preparation of solution, thin film deposition and lastly followed by the encapsulation of the device. After that, the methodology in the characterization's measurements were presented. Electrical, optical, HOMO-LUMO determination, surface roughness and morphological studies are the presented characterization's measurements involved in this study. Figure 3.1 shows the flow chart of the fabrication and characterization measurements of OPD devices involved in this study.

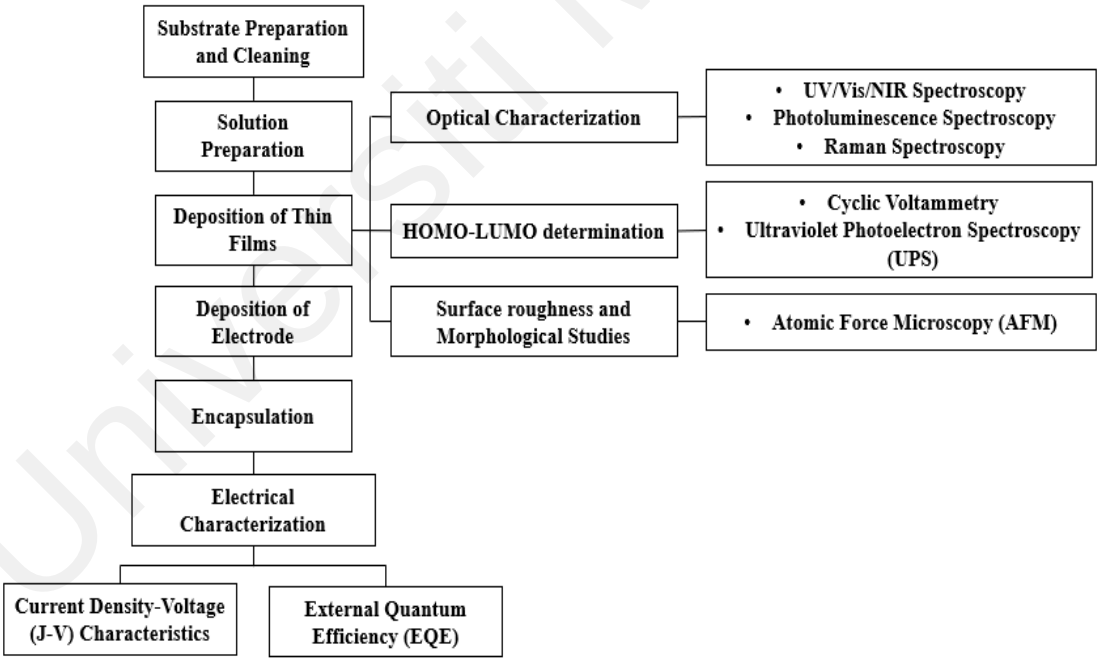

Figure 3.1: The flow of methodology in the device fabrication and characterization measurements.

3.1 Substrate Preparation and Cleaning

Glass, patterned and blank indium-tin oxide (ITO)-coated glass substrates has been used in this study for the utilization in the measurement's characterization. The glass substrate is usually used for optical characterization as an initial measurement to understand the blend composition. Blank coated ITO glass substrate, however is used for the electrochemical, surface roughness and morphological studies. Blank ITO acts as a working electrode (WE) in the electrochemical measurements. Meanwhile, patterned coated ITO glass substrate used in the fabrication of OPD as a transparent conductive electrode that allows light to pass through. Figure 3.2 shows the geometric drawing of patterned coated ITO glass substrate. The geometric design illustrates the patterned ITO substrate which contains 6 pixels with 0.045 cm^2 (1.5 mm x 3 mm) of active area in each pixel.

Substrates cleaning process is required to form a homogeneous and smooth thin film in the fabrication of OPD devices. The non-smooth and contaminated substrates will affect the performance of OPD by changing their properties. Thus, a proper cleaning method is a must in the fabrication of OPD as an assurance to the accuracy of the results. A normal cleaning method can be done by sequentially cleaning in an ultrasonic bath with soap water, deionized (DI) water, acetone, isopropanol, and again DI water for 15 min each. Then, the substrates are dried up with nitrogen purge before UV-ozone treatment for another 5 min.

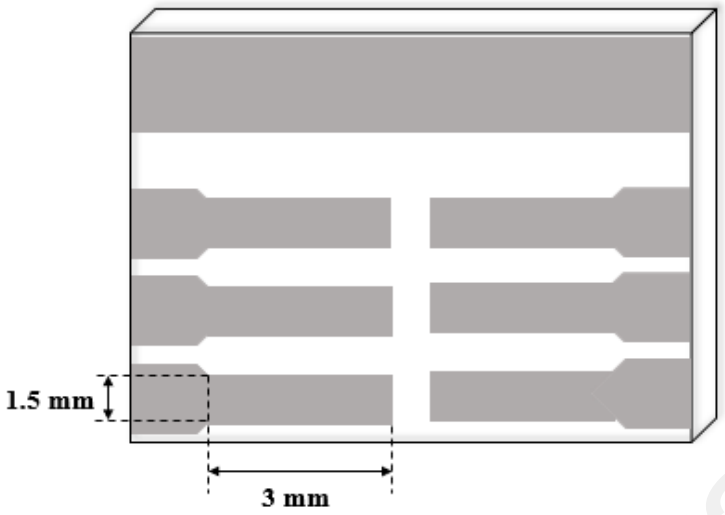

Figure 3.2: The geometric drawing of patterned coated ITO glass substrate.

3.2 Solution preparation

Vanadyl 2,11,20,29-tetra-tert-butyl-2,3-naphthalocyanine (VTTBNc) and [6,6]phenyl-C61-butyric acid methyl ester ($PC_{61}BM$) were purchased from Sigma Aldrich. Meanwhile, [6,6]phenyl-C71-butyric acid methyl ester ($PC_{71}BM$) was procured from Luminescence Technology Corp. (Taiwan). In the preparation of solution for the active component, the 20 mg of VTTBNc, $PC_{61}BM$ and $PC_{71}BM$ was dissolved separately in 1mL chloroform and stirred overnight. This process was done in the nitrogen-filled glove box. Figure 3.3 shows the nitrogen-filled glove box used in this study. Both materials $PC_{61}BM$ and $PC_{71}BM$ act as electron acceptors, while VTTBNc acts as an electron donor. Then, the solution has been filtered with the nylon filter of membrane pore size 0.20μm before the solution is subjected to the deposition process. In the preparation of a blend solution with different stoichiometric ratio, VTTBNc was mixed in each $PC_{61}BM$ and $PC_{71}BM$ in three different volume ratios (1:0.5, 1:1.0, 1:1.5) as shown in Table 3.1.

Table 3.1: The blend ratio of the blend solution involved.

Blend solution	Volume ratios
VTTBNc:$PC_{61}BM$	1:0.5, 1:1.0, 1:1.5
VTTBNc:$PC_{71}BM$	1:0.5, 1:1.0, 1:1.5

Figure 3.3: The nitrogen-filled glove box by MIKROUNA Super (1500/750).

3.3 Deposition of thin film by spin coating technique

The spin coating process has been performed for the deposition of thin films using a spin coater (Laurell WS-650MZ-23NPP) as shown in Figure 3.4. Spin coating is an industry-leading method for depositing thin films of materials onto the functional substrate. It uses centrifugal force as the method for the deposition of the thin film. The thickness of the thin film formed using this method ranges from just a few micrometres (μm) down to a single nanometre (nm). This method operates by controlling the speed based on the material properties relative to the solution. Viscosity is the main property as it determines the resistance of the solution to flow uniformly, which is essential for achieving uniform surface finish.

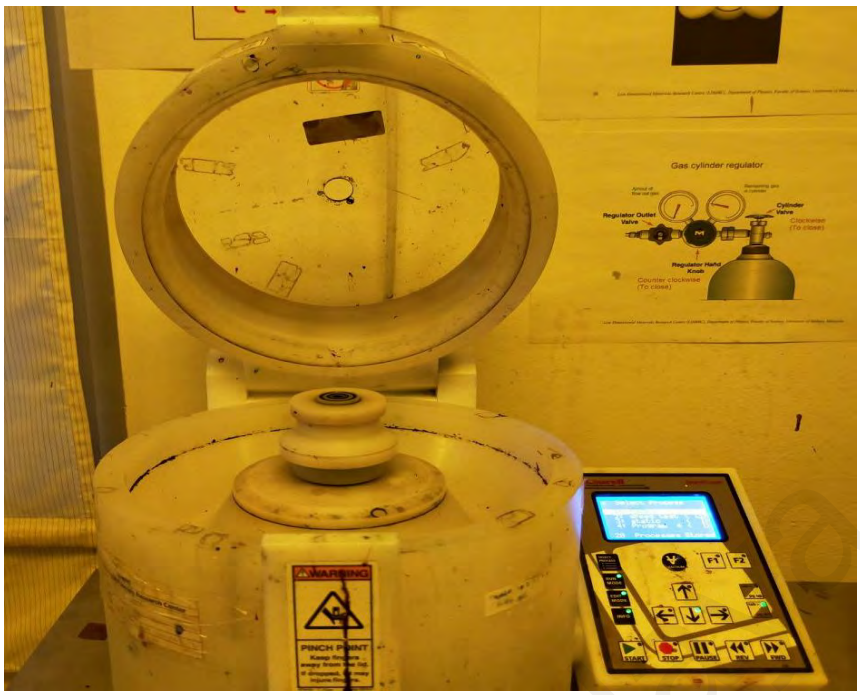

Figure 3.4: Spin coater by Laurell model WS-650MZ-23NPP.

The process of thin film's deposition was initially started by putting the substrate on the top of the rotation platform in the spin coater. Then, the substrate was sucked by suction on the rotation platform by turning on the vacuum pump. By using a syringe, a small amount of the solution was dispensed onto the substrate. Immediately after that, the spin coater started spinning as the button start was pressed. During the spinning, the fluid starts to thin based on the viscous force and the solvent volatility of the blend solution. The rotation speed and the duration of spinning was set up before the spin coating process began. Figure 3.5 illustrates the spin coating process for thin film deposition.

In this work, spin coating has been used to deposit hole transport layers and the photoactive layers. The hole transport layer used in this study is poly(3,4-ethylenedioxythiophene) polystyrene sulfonate (PEDOT:PSS, PH1000) and was purchased from H.C Stack. The photoactive layers are deposited from the blended solution that has been prepared. Before the spin coating process, the PEDOT:PSS has been filtered using 0.45μm nylon filter and spin coated at 3000 rpm for 60s on top of pre-cleaned ITO substrate. The PEDOT:PSS layer was annealed for 30 min at 130 ℃, to

completely evaporate the solvent. Meanwhile, the photoactive layer was spun at 2000 rpm for about 30 seconds and annealed for 30 min at 110 ℃ to form a 146 nm thickness layer. The photoactive layer deposition has been conducted in the nitrogen-filled glove box.

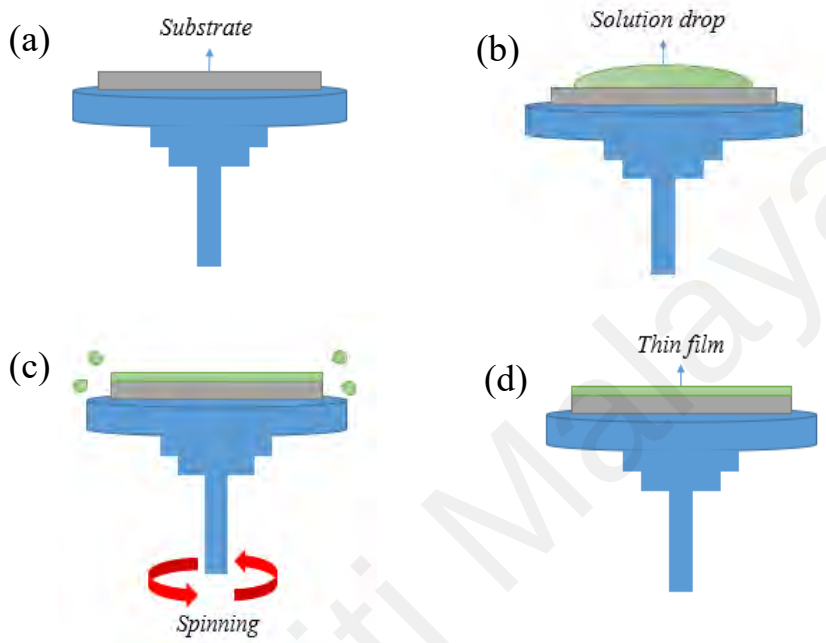

Figure 3.5: Spin coating process. (a) Substrate placing. (b) Solution drops onto the substrate. (c) Spinning of spin coater. (d) Formation of thin film.

3.4 Deposition of electrode by thermal evaporation process

The deposition of electrodes (Aluminium) was done through the evaporation process. This technique is one of the common methods of physical vapor deposition (PVD). In this process, a thin film is formed using a resistive heat source that has been applied to evaporate a solid material under high vacuum conditions. Subsequently, the vaporized material is transported to the vacuum chamber by thermal energy and coats the substrate.

The thermal evaporator located inside the glove box is used to deposit Aluminium (Al). A base pressure of $2x10^{-7}$ torr has been applied to the thermal evaporator under a control of the evaporation rate to deposit 100 nm Aluminium. During the deposition, the shadow mask as shown in Figure 3.6 has been used. Finally, the OPD devices were

encapsulated with the glass using epoxy glue and cured under UV light. The purpose of encapsulation is to extend the device performance and the stability of the OPD from being oxidized. Figure 3.7 shows the fabricated OPD device.

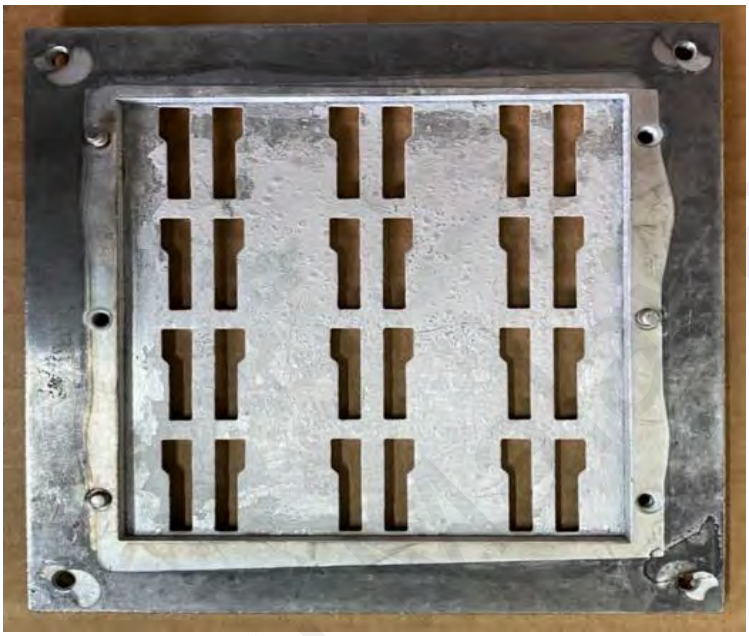

Figure 3.6: The shadow mask used for the deposition of Aluminium.

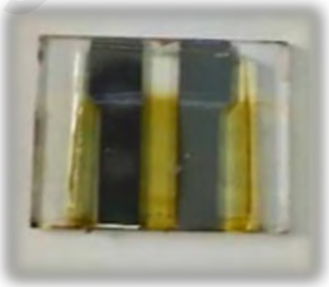

Figure 3.7: The fabricated OPD device.

3.5 Electrical characterization

3.5.1 J-V characteristics

The current density-voltage (J-V) characteristics of the OPD were measured using a Keithley 236 Source Measure Unit (SMU) equipped with an Oriel (Xenon arc lamp) solar simulator with an illumination of 100 mW/cm^2 input power. This measurement has been conducted under ambient conditions in a dark box. The dark box was used to effectively obstruct the background light from the outside. The sample was connected to the SMU using the sample holder which probes to the anode and cathode. A *LabVIEW* J-V programme has been employed to display the data result.

3.5.2 EQE

External Quantum Efficiency (EQE) was acquired from the PVE300 Photovoltaic EQE (IPCE) system. The IPCE system measured the EQE efficiency and responsivity in the wavelength range from 350 nm to 1050 nm.

3.6 Optical characterization

3.6.1 Ultraviolet/Visible/Near-Infrared (UV/VIS/NIR) spectroscopy

The UV/Vis/NIR spectroscopy has been conducted to characterize the photoactive layers' absorption spectra. The measurement is done by counting the intensity of light that passes through a sample with respect to the reference sample using a spectrophotometer. The spectrophotometer involved in this work was a Perkin Elmer LAMBDA 900 spectrophotometer as shown in Figure 3.8. In the spectrophotometer, there are two substrate holders provided. One of them is used for the baseline calibration and the other one is used to characterize the absorption spectroscopy of organic thin film. The organic thin films for this characterization have been prepared by the deposition of the photoactive layer onto the glass substrate. At the beginning of the measurements, a baseline correction has been performed by placing two uncoated substrates on the sample

holders in order to remove the background absorption spectrum. After that, one of the uncoated substrates has been replaced with the deposited organic thin film substrate. The absorption spectra of the organic thin film are then measured by a spectrophotometer with the uncoated substrate as a reference.

Figure 3.8: Perkin Elmer LAMBDA 900 spectrophotometer.

3.6.2 Photoluminescence (PL) spectroscopy

Photoluminescence (PL) spectroscopy is a non-contact, non-destructive method for detecting the electronic structure of materials. In this measurement, the sample is induced by the photon, and subsequently stimulates the emission of a photon as the excess energy received into the material. This occurrence is called photo-excitation that causes the electron in the organic material to jump to the LUMO level and then emits the energy when the material relaxes back to a lower energy level. This illumination of the photon energy from the material is the process that occurred in the PL spectroscopy measurement.

In this work, the PL spectroscopy has been analysed by using Renishaw inVia Raman microscope under 325nm excitation wavelength. Samples of the thin film deposited onto the glass substrate are used for the characterization of PL spectroscopy.

3.6.3 RAMAN spectroscopy

Raman spectroscopy is based on the interaction between light and chemical bonds in the material. It is known as a non-destructive chemical analysis method which accommodates information on the material chemical structure, molecular interaction, phase, crystallinity and polymorphism. The interaction of light with molecules will cause the scattering of photons. Most of the scattered photons are at the same energy as the incident light induced to the molecule. This scattering can be called a Rayleigh scattering. In Raman spectroscopy, a laser source is provided for interacting light to the molecule. The Raman spectra show the intensity and wavelength position of the peaks that correspond to the specific molecular vibration, individual bonds and groups of bonds of the material.

For this experiment, a Renishaw inVia Raman microscope is used for the study of chemical structure in Raman spectroscopy. The samples for the characterization have been prepared using a deposited photoactive layer onto the glass substrate. A laser source with 532 nm wavelength has been used to investigate the Raman spectroscopy of the organic thin films.

3.7 HOMO-LUMO determination

Cyclic voltammetry (CV) and Ultraviolet Photoelectron Spectroscopy (UPS) has been used to determine the HOMO-LUMO energy levels of the donor material which is VTTBNc.

3.7.1 Cyclic Voltammetry (CV)

Cyclic Voltammetry (CV) is a useful electrochemical technique that measures the current response to the linear cycle of the potential applied in an electrochemical cell. The current response of the electrochemical cell provides information on the redox couple in which the reduction and oxidation process occurred. In CV, the first oxidation and the

first reduction of the material obtained from the CV is often correlated with the HOMO and LUMO energy levels. This energy level can be determined by measuring the oxidation and reduction onset of the study material. The HOMO and LUMO energy levels can be calculated based on the equation below:

$$HOMO/LUMO = -e(E_{OX/RED} + 4.4) \quad (3.1)$$

Where E_{OX} and E_{RED} are the onset potential for oxidation and reduction, respectively. Meanwhile, 4.4 V is the potential of standard hydrogen electrode (SHE) on the absolute vacuum scale (Peljo & Girault, 2018; Trasatti, 1986).

In the CV system, three electrodes are used to generate the current response. The electrodes used consist of a working electrode (WE), reference electrode (RE), and counter electrode (CE). The electrodes involved in this work are platinum as a CE, Ag/AgCl as a RE and ITO as a WE. For the ion's migration of the redox process, the electrolyte solution has been prepared using 0.01M hydroquinone in HCl with pH 3. The thin films of the study materials are readily prepared by the deposition of VTTBNc onto the blank ITO coated glass with dimension 2 x 1 cm^2. A Nova 1.11 has been utilized to display the result of the CV.

3.7.2 Ultraviolet Photoelectron Spectroscopy (UPS)

Ultraviolet photoelectron spectroscopy (UPS) is the measurement to determine the molecular orbital energies in the valence band (HOMO). In UPS, ultraviolet (UV) light is generated using a gas discharge lamp. Then, the thin film surface irradiates the UV light which has been absorbed by the molecules. The determination of HOMO level can be calculated by the following equation:

$$Work\ function = hv - Cuttoff\ energy \quad (3.2)$$

$$HOMO = Work\ function + HOMO_{onset} \quad (3.3)$$

Where *hv* is the energy of an incident photon. In this work, the thin film samples have been prepared by spinning and casting the photoactive layer onto the blank ITO substrate. The ULVAC-PHI500 VersaProbe II is used to analyse the UPS spectra. The UPS result shows that the intensity gain varied by the binding energy.

3.8 Surface roughness and Morphological studies

3.8.1 Atomic Force Microscopy (AFM)

Atomic force microscopy (AFM) is the most powerful and versatile microscopy technology for studying samples at the nanoscale. The versatility of AFM cannot be disputed as it provides the details of three-dimensional topography and various types of surface measurements. The atomic resolution of the AFM images results in a powerful resolution with an angstrom scale, even with only a minimum sample preparation.

The Hitachi AFM5100 using S1-DF3 cantilever has been used in this study for the investigation of the surface roughness and morphology on the thin film surface. A cantilever is used in AFM to scan the sample surface over a region of interest. The thin film samples used in this experiment are the deposited photoactive layer using blank ITO substrates.

CHAPTER 4: RESULTS AND DISCUSSION

4.0 Overview

Chapter 4 discussed the experimental results based on the OPD performance and the photoactive layer characterization. The first part of this chapter is focussed on the discussion of absorption of the photoactive materials and the determination of VTTBNc's HOMO-LUMO level. Next, the performance of the OPD has been analysed based on the result obtained in the electrical characterization. In this study, the electrical characterization was carried out by the measurement of J-V characteristics and EQE which stated in chapter 3. Lastly, further discussion in the characterization of photoactive layers which includes photoluminescence spectroscopy, RAMAN spectroscopy and AFM images has been explained on the basis of device performance obtained.

4.1 The characterization of photoactive layer thin films

4.1.1 Absorption Characteristics

Figure 4.1 shows the absorption spectra of the UV-Vis region of the single component material and the blended films from 300 nm to 900 nm wavelength range. Figure 4.1(a) illustrates the absorption spectra of the single component materials which are VTTBNc, $PC_{61}BM$ and $PC_{71}BM$. It is observed that VTTBNc exhibits two broad peaks at B-band (333 nm) and Q-band region (761 nm and 810 nm). These absorption peaks are similar to the absorption spectra reported by Dhanya and Menon (2012) indicating that electronic transition of π-π* excitation occurred between bonding and anti-bonding (Dhanya & Menon, 2012). Meanwhile, $PC_{61}BM$ reveals a maximum absorption peak located at 335 nm and $PC_{71}BM$ has several shoulder peaks observed at 373 nm and 473 nm as illustrated in Figure 4.1(a). The illustration of Figure 4.1(a) suggested that $PC_{71}BM$ has a stronger

and wider absorption range in the visible spectrum compared to $PC_{61}BM$. This is due to the less symmetrical in $PC_{71}BM$ that relaxed the forbidden transitions in longer wavelengths that form in $PC_{61}BM$ (Arbogast & Foote, 1991; Benatto et al., 2020). Besides, by replacing $PC_{71}BM$, the degeneracy of the electronic states has reduced and led to the increase in the electronic state's density which corresponds to the number of allowed transition states (Orlandi & Negri, 2002).

Figure 4.1(b) and (c) illustrate the absorption of the binary blend of VTTBNc:$PC_{61}BM$ and VTTBNc:$PC_{71}BM$, respectively. Both graphs show a binary blend of VTTBNc:$PC_{61}BM$ and VTTBNc$PC_{71}BM$ exhibit a broader absorption spectrum. The absorption using an acceptor $PC_{71}BM$ diminished the broader valley between 384 nm to 639 nm in VTTBNc. Meanwhile, $PC_{61}BM$ only diminished the valley between 460 nm to 618 nm. Thus, these elucidates that blend using $PC_{71}BM$ have a stronger absorption in the visible range compared to the blend with $PC_{61}BM$. Both VTTBNc:$PC_{61}BM$ and VTTBNc:$PC_{71}BM$ differ in three volumetric ratios. At the Q-band region, all blend ratios with the least amount of electron acceptor exhibit higher absorption due to the high volume of VTTBNc towards the blend. VTTBNc:$PC_{61}BM$ shows almost the same level of absorption intensity at the shorter wavelength. While in VTTBNc:$PC_{71}BM$, 1:0.5 shows a significant peak at 328 nm in the UV region. The significant peak in VTTBNc:$PC_{71}BM$ (1:0.5) may be due to the least amount of $PC_{71}BM$ that led to the significant VTTBNc peak. In the visible range (450-620 nm), VTTBNc:$PC_{71}BM$ observed the increase in intensity with increasing $PC_{71}BM$ composition.

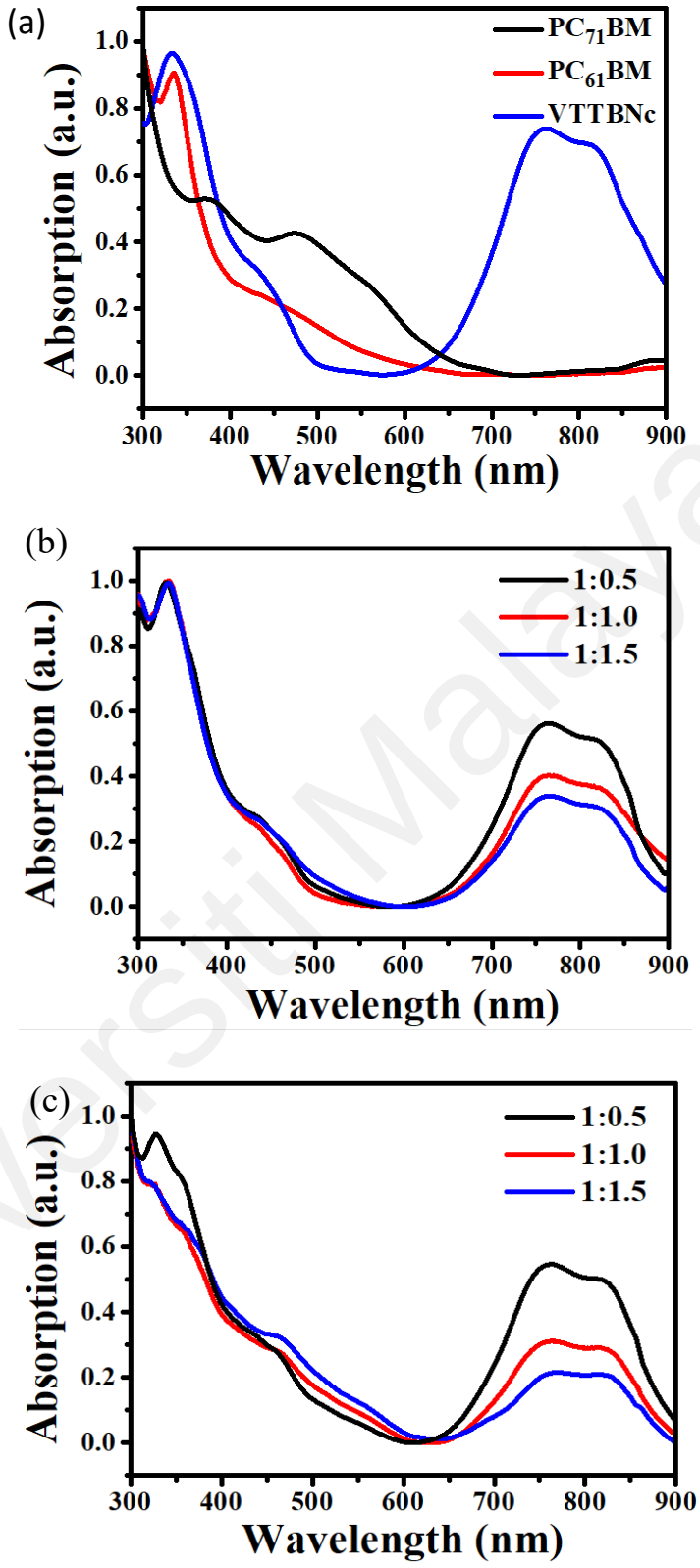

Figure 4.1: (a) Absorption spectra of VTTBNc, $PC_{61}BM$ and $PC_{71}BM$ thin films. Absorption spectra of (b) VTTBNc:$PC_{61}BM$ and (c) VTTBNc:$PC_{71}BM$ of different volumetric ratios.

4.1.2 Determination of VTTBNc Energy Band Gap

One of the most widely applied techniques for the determination of optical band gap is using a UV-Vis absorption spectrum with the combination of Tauc plot technique (Tauc, Grigorovici, & Vancu, 1966). The optical band gap energy can be determined according to Tauc technique by simply extrapolating a line to the linear region of the absorption spectrum. From the Tauc plot shown in Figure 4.2, the optical band gap energy of VTTBNc is measured as 1.36 eV at Q-band region. This result is slightly low compared to the band gap reported by Dhanya and Menon (2012) which is between 1.7 eV and 1.8 eV (Dhanya & Menon, 2012). Besides, the Q-band gap energy has been chosen due to half of the solar photon flux occurring at the low band gap energy and essential in the development of NIR OPD (Pandey et al., 2013).

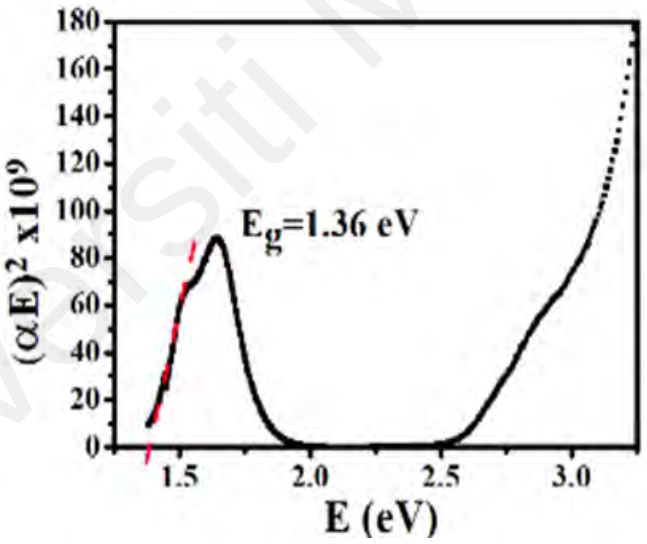

Figure 4.2: Absorption spectrum Tauc plot of VTTBNc thin film.

Referring in Figure 2.1(a), VTTBNc has large aromatic π-system that enables stronger absorption in the NIR (810 nm) region. This characteristic leads to a low band gap of the material. The low band gap also results in a smaller energy offset between HOMO or LUMO of the donor and acceptor material. This allows the reduction in open-circuit voltage loss by minimizing the loss caused by charge transfer state between donor-

acceptor (Cheng & Yang, 2020). The utilization of the absorption in the NIR region was expected to enhance the photocurrent of the device. It is also suitable to make transparent OPD with high transmittance in visible regions by utilizing such high NIR-absorbing materials.

4.1.3 HOMO-LUMO determination of VTTBNc

Cyclic voltammetry (CV) and Ultraviolet Photoelectron Spectroscopy (UPS) are used in the determination of HOMO-LUMO levels.

Cyclic Voltammetry (CV)

Figure 4.3(a) depicts the CV of VTTBNc at different scan rates and Figure 4.3(b) shows the CV of measured current vs applied potential for bare ITO and VTTBNc at scan rate of 75 mV/s. Meanwhile, Table 4.1 shows the oxidation and reduction onset potential at different scan rates. The potential difference of oxidation and reduction potential is always correlated with the electrochemical band gap. The oxidation and reduction onset potential has been determined based on the first oxidation and reduction peak of VTTBNc with reference to the bare ITO. From the CV plots, it is observed that VTTBNc altered the oxidation and reduction peak if compared with the bare ITO. The difference in onset potential at 75 mV/s observed the closest value with the band gap value obtained in the optical system (1.36 eV). Besides, the scan rate of 75 mV/s reveals the most prominent reduction peak compared to other scan rates as shown in Figure 4.3(a). Thus, a scan rate of 75 mV/s has been chosen as the optimized scan rate in the determination of HOMO-LUMO levels in VTTBNc.

The onset potential for oxidation and reduction of scan rate of 75 mV/s is observed at 0.742 V and -0.662 V, from Figure 4.3(b). These values of HOMO-LUMO levels were found to be as -5.14 eV and -3.74 eV. Based on the difference in HOMO-LUMO levels, the band gap energy of 1.4 eV is obtained from the CV technique. The value of band gap

energy obtained from CV (1.4 eV) is almost the same as the optical band gap energy which is recorded as 1.36 eV. This suggests a small interface barrier between electrode and VTTBNc thin film in the CV system and gives rise to the equilibrium state occurring quickly (Elgrishi et al., 2018; Misra et al., 2005). Figure 4.4 shows the illustration of energy levels of VTTBNc obtained in CV with respect to the fullerene derivatives. The HOMO-LUMO energy levels of $PC_{61}BM$ and $PC_{71}BM$ are obtained from the reference (Schulz et al., 2013).

Table 4.1: The oxidation and reduction onset potential at different scan rates.

Scan rate (mV/s)	Oxidation onset potential (V)	Reduction onset potential (V)	Potential difference (V)
50	0.852	-0.670	1.522
75	0.742	-0.662	1.404
100	0.724	-0.766	1.490

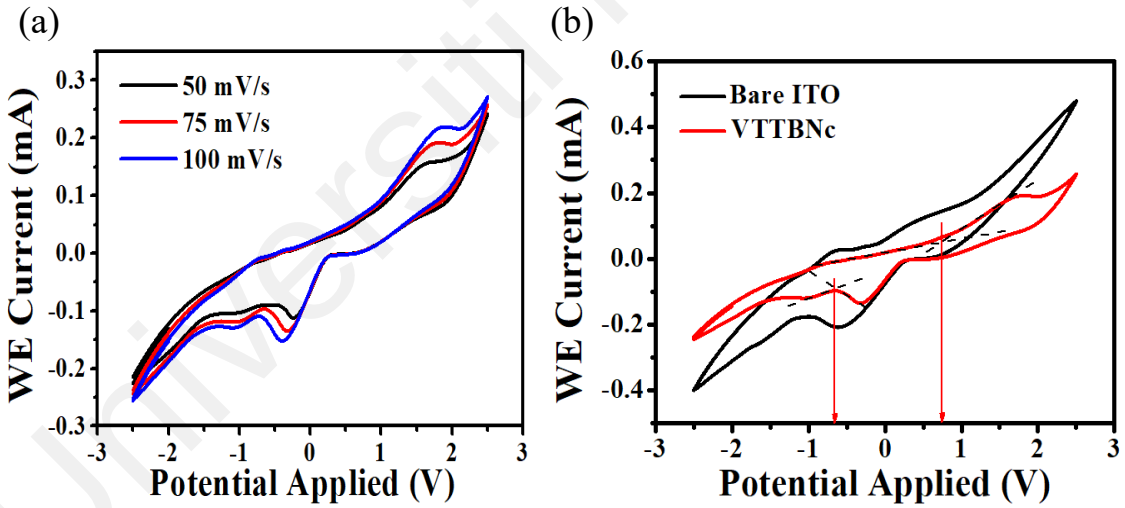

Figure 4.3: Cyclic Voltammogram (CV) of measured current versus applied potential in VTTBNc at (a) different scan rate and (b) at scan rate 75 mV/s with reference to the bare ITO.

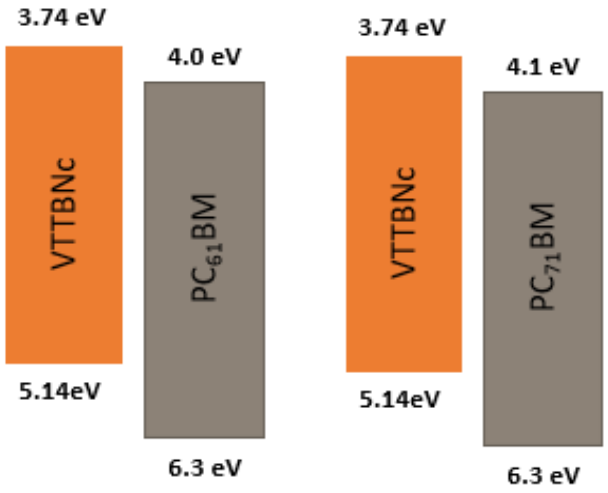

Figure 4.4: The illustration of VTTBNc's energy level obtained in CV with respect to the fullerene derivative.

Ultraviolet photoelectron spectroscopy (UPS)

Figure 4.5 shows the UPS spectra for the determination of VTTBNc's HOMO level. From UPS spectra, $HOMO_{onset}$ and cut-off energy of VTTBNc are observed at 0.70 eV and 35.06 eV, respectively. Through these values, the HOMO level can be calculated using equation (3.2) & (3.3) in chapter 3. The work function of 4.44 eV was obtained from the energy of an incident photon and cut-off energy observed in UPS spectra (39.50 eV – 35.06 eV). Thus, by using the work function and the $HOMO_{onset}$ observed in the UPS spectra, the HOMO level of 5.14 eV has been obtained. Then, the position of LUMO level has been determined from the optical band gap observed in the Tauc plot. In the naphthalocyanine types of material, the extended aromatic system cause in the destabilization of HOMO level with respect to LUMO level in which the mobilization of π electrons occurred (Dubinina et al., 2020). Even though the aromatic system in the naphthalocyanine lead to greater distribution of energy in the molecule which result in higher stability when exposed to atmospheric oxygen (Dubinina et al., 2020). Table 4.2 shows the observed and calculated values in determining HOMO-LUMO levels of

VTTBNc and Figure 4.6 show the illustration of energy levels of VTTBNc obtained in UPS with respect to the fullerene derivatives.

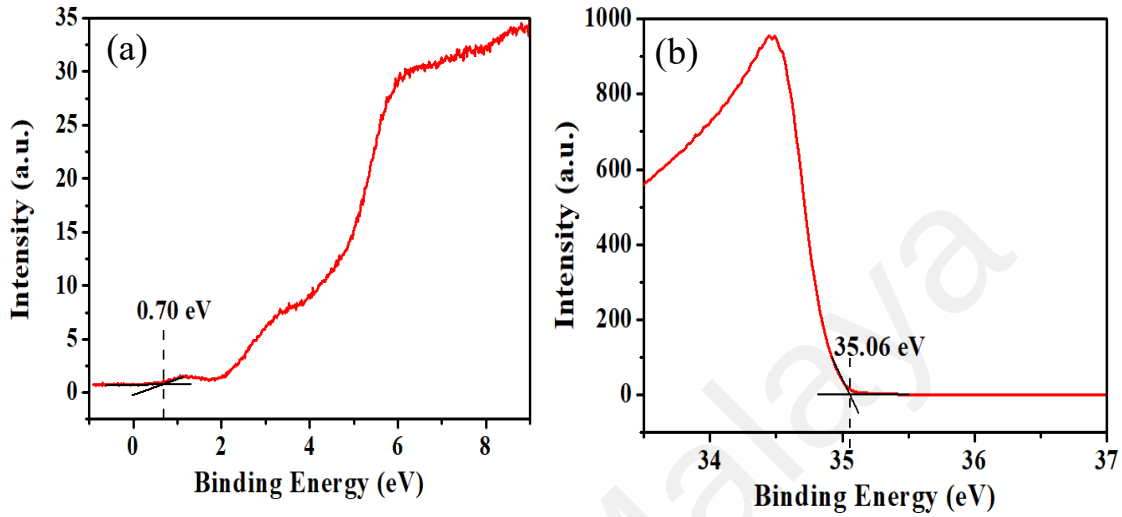

Figure 4.5: The measured UPS spectra showing (a) HOMO onset and (b) cut-off energy for the determination of VTTBNc's HOMO level.

Table 4.2: The observed and calculated values involved in UPS for determination of HOMO-LUMO levels of VTTBNc.

HOMOonset (eV)	0.70
Cut-off energy (eV)	35.06
Work function (eV)	4.44
HOMO level (eV)	5.14
E_g (eV)	1.36
LUMO level (eV)	3.78

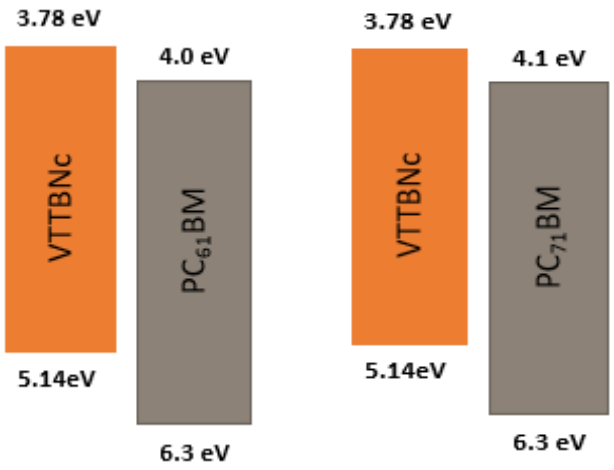

Figure 4.6: The illustration of VTTBNc's energy level obtained in UPS with respect to the fullerene derivative.

CV versus UPS

In CV, the HOMO-LUMO levels can be determined from the redox couple in which the oxidation and reduction process occurred. UPS is measured based on the photoemission onset energy in the determination of HOMO level. Since the LUMO level is unavailable in UPS measurement, then a common method is used by combining the HOMO from UPS and the optical band gap energy for the determination of LUMO level. In this study, a good correlation in HOMO level has been obtained for both methods as they exhibit the same value of HOMO which is 5.14 eV. While LUMO levels for both methods were slightly different which are 3.74 eV for CV and 3.78 eV for UPS. This uncertainty corresponds to the difference in the band gap energy involved in the determination of LUMO levels. The electrochemical band gap energy (1.4 eV) is slightly larger than the optical band gap energy (1.36 eV) which results in the LUMO levels of both methods having a slight difference of 0.04 eV. This difference is indicated by a small interface barrier between electrode and VTTBNc thin film that exists in the CV system. However, due to the similarity of electrochemical processes with charge transport in OPD, the electrochemical band gap is a more significant approach in the evaluation of HOMO-LUMO levels compared to the optical band gap (Misra et al., 2005). Figure 4.7

shows the illustration of energy levels of each material that included the work function and HOMO-LUMO of the OPD devices. The proper alignment of HOMO-LUMO energy levels between the donor and acceptor is essential for the charge separation in an OPD device.

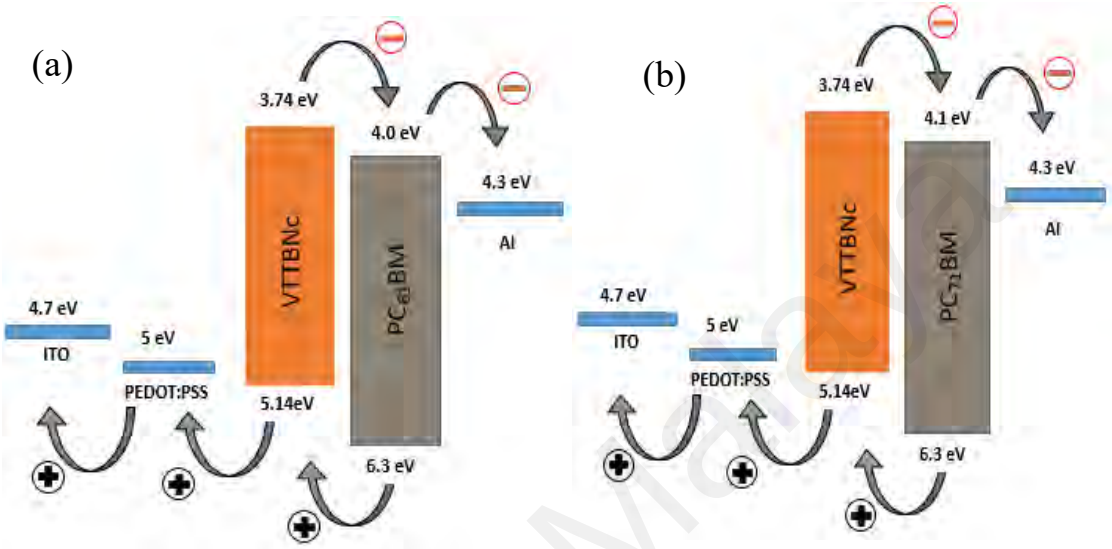

Figure 4.7: The HOMO-LUMO energy levels and work function for the OPD devices. (a) ITO/PEDOT:PSS/VTTBNc:$PC_{61}BM$/Al. (b) ITO/PEDOT:PSS/VTTBNc:$PC_{71}BM$/Al.

4.2 The performance of the OPD devices

4.2.1 J-V Profiles

As seen in Figure 4.8, it is observed that $PC_{71}BM$ generated high photocurrent that exhibits higher responsivity compared with $PC_{61}BM$ when the voltage was applied. The responsivity of $PC_{71}BM$/$PC_{61}BM$ is measured as (16.40/10.50) mA/W, (20.66/14.32) mA/W, (21.20/16.21) mA/W at 0 V, -0.5 V, -1 V bias respectively, as listed in Table 4.3. $PC_{71}BM$ devices have higher photocurrent generation due to strong absorption in the visible region as observed in Figure 4.1. However, high dark current observed in $PC_{71}BM$ devices causes the device to have lower detectivity at reversed bias compared to $PC_{61}BM$. The high dark current in $PC_{71}BM$ may be due to the high thermal generation of charge

carriers at the contacts as the voltage applied (Simone, Dyson, Meskers, Janssen, & Gelinck, 2019).

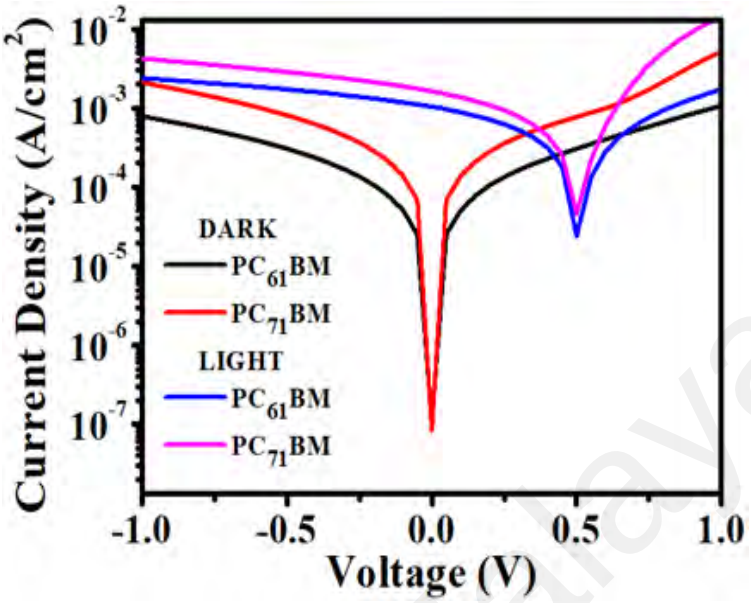

Figure 4.8: J-V characteristics of $PC_{61}BM$ and $PC_{71}BM$ under dark and light illumination.

Table 4.3: Performance of $PC_{61}BM$ and $PC_{71}BM$ as a photodiode.

Sample	Bias (V)	J_D (A/cm^2)	J_{ph} (A/cm^2)	R (mA/W)	D* (Jones)	V_{OC} (V)
$PC_{61}BM$	0	1.04×10^{-7}	1.05×10^{-3}	10.50	5.75×10^{10}	0.5
	-0.5	3.08×10^{-4}	1.74×10^{-3}	14.32	1.44×10^{9}	
	-1.0	7.89×10^{-4}	2.41×10^{-3}	16.21	1.02×10^{9}	
$PC_{71}BM$	0	8.42×10^{-8}	1.64×10^{-3}	16.40	9.98×10^{10}	0.5
	-0.5	8.14×10^{-4}	2.88×10^{-3}	20.66	1.28×10^{9}	
	-1.0	2.15×10^{-3}	4.27×10^{-3}	21.20	8.08×10^{8}	

In order to improve the OPD performance, VTTBNc as a p-type material is blended with each $PC_{61}BM$ and $PC_{71}BM$. Figure 4.9(a) & (b), shows the measured current density versus applied voltage for three different ratios of VTTBNc:$PC_{61}BM$ and VTTBNc:$PC_{71}BM$. The result shows that the highest content (1:1.5) of $PC_{61}BM$ in VTTBNc:$PC_{61}BM$ has the highest measured responsivity and detectivity. In the case of VTTBNc:$PC_{71}BM$ blend, ratio 1:1.0 has shown the highest detectivity of 3.85×10^{11} Jones and 2.31×10^{9} Jones at 0 V and -1 V, respectively. On the other hand, the ratio of 1:1.5

exhibits lower detectivity of 8.48×10^{10} Jones and 2.05×10^{9} Jones while higher in the responsivity at 9.55 mA/W and 28.48 mA/W at 0 V and -1 V, respectively. The high detectivity of ratio 1:1.0 may be due to the low value of the dark current density obtained. A low value of the dark current is favorable in photodetection application as it indicates low noise and high detectivity in the OPD device. High dark current will lead to higher device power consumption and may accommodate the photodiode to hardly detect weak signals for signal readout (Natali & Caironi, 2016). Thus, the device with a ratio 1:1.0 was considered as an optimized device in VTTBNc:$PC_{71}BM$ as it has the highest detectivity values. As compared between these two blended materials, VTTBNc:$PC_{71}BM$ seems to have the highest responsivity and detectivity values. As seen in Table 4.4, the responsivity measured for optimized ratio of VTTBNc:$PC_{71}BM$ (1:1.0) and VTTBNc:$PC_{61}BM$ (1:1.5) are (6.96/3.63) mA/W, (15.04/7.38) mA/W, and (26.11/10.89) mA/W at 0 V, -0.5 V, and -1 V, respectively. On the other hand, the detectivity for both optimized devices are (3.85×10^{11}/4.41×10^{9}) Jones, (2.37×10^{9}/1.53×10^{9}) Jones, and (2.31×10^{9}/1.21×10^{9}) Jones at 0 V, -0.5 V and -1 V, respectively. Figure 4.10 depicts the trend in detectivity and responsivity of the optimized ratio in VTTBNc:$PC_{61}BM$ and VTTBNc:$PC_{71}BM$. According to detectivity values obtained in Table 4.3 & Table 4.4, it is evident that the addition of VTTBNc has greatly improved the detectivity limit in VTTBNc:$PC_{71}BM$ device to about 186% with respect to $PC_{71}BM$-only device compared to VTTBNc:$PC_{61}BM$ device which increases only around 19% with respect to $PC_{61}BM$-only device.

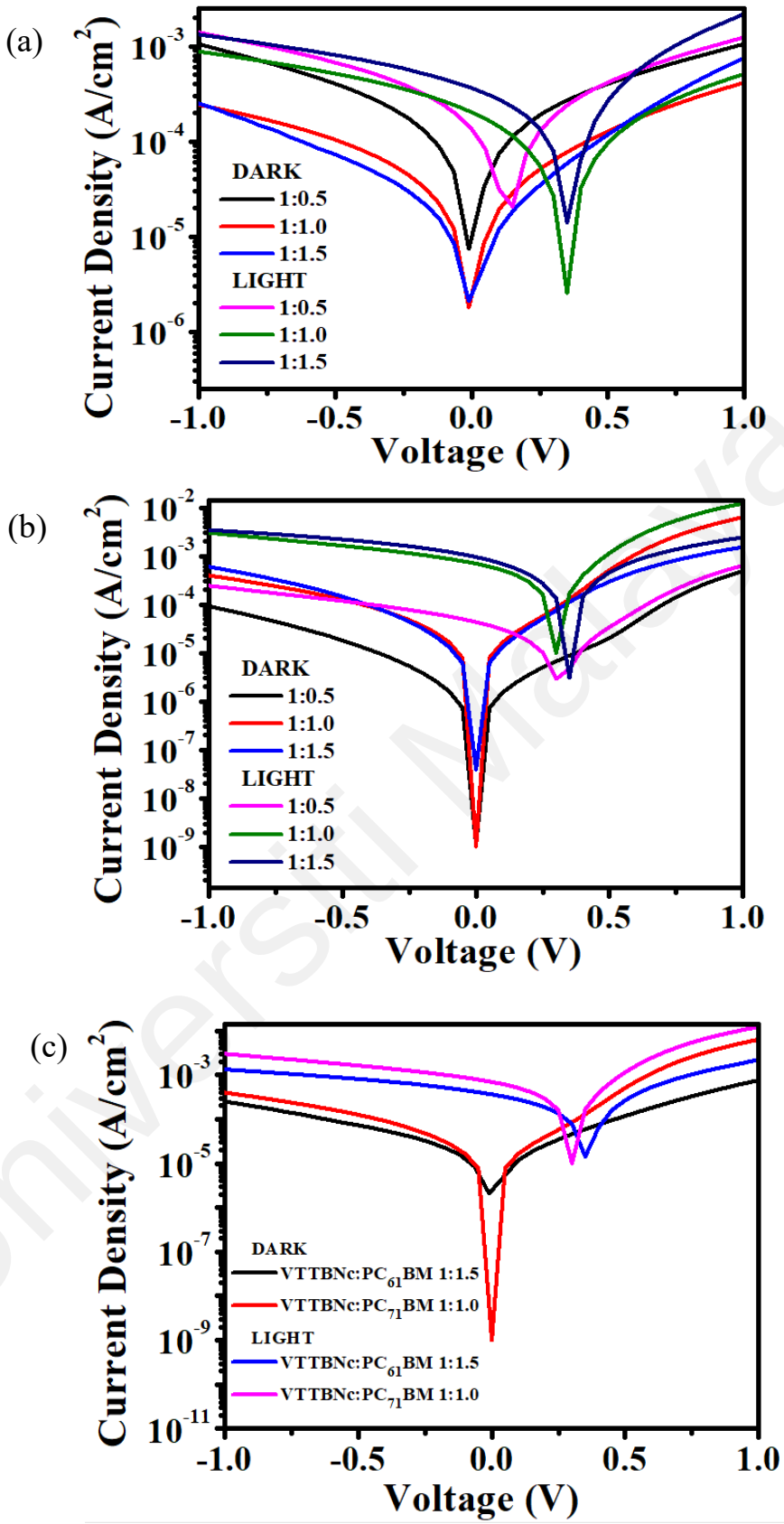

Figure 4.9: J-V characteristics of (a) VTTBNc:PC$_{61}$BM and (b) VTTBNc:PC$_{71}$BM of different ratios. J-V characteristics of (c) VTTBNc:PC$_{61}$BM and VTTBNc:PC$_{71}$BM of the optimized ratios.

Table 4.4: Performance of VTTBNc:$PC_{61}BM$ and VTTBNc:$PC_{71}BM$ as a photodiode.

	Ratio	Bias (V)	J_D (A/cm^2)	J_{ph} (A/cm^2)	R (mA/W)	D* (Jones)	V_{OC} (V)
VTTBNc:$PC_{61}BM$	1:0.5	0	7.48×10^{-6}	1.35×10^{-4}	1.28	8.24×10^{8}	0.15
		-0.5	4.13×10^{-4}	6.75×10^{-4}	2.62	2.28×10^{8}	
		-1.0	1.06×10^{-3}	1.40×10^{-3}	3.40	1.84×10^{8}	
	1:1.0	0	1.82×10^{-6}	2.03×10^{-4}	2.01	2.64×10^{9}	0.35
		-0.5	1.07×10^{-4}	5.17×10^{-4}	4.10	7.00×10^{8}	
		-1.0	2.43×10^{-4}	8.84×10^{-4}	6.41	7.26×10^{8}	
	1:1.5	0	2.11×10^{-6}	3.65×10^{-4}	3.63	4.41×10^{9}	0.35
		-0.5	7.27×10^{-5}	8.11×10^{-4}	7.38	1.53×10^{9}	
		-1.0	2.51×10^{-4}	1.34×10^{-3}	10.89	1.21×10^{9}	
VTTBNc:$PC_{71}BM$	1:0.5	0	1.08×10^{-9}	4.35×10^{-5}	0.43	2.34×10^{10}	0.3
		-0.5	1.81×10^{-5}	1.18×10^{-4}	1.00	4.15×10^{8}	
		-1.0	9.25×10^{-5}	2.43×10^{-4}	1.51	2.76×10^{8}	
	1:1.0	0	1.02×10^{-9}	6.96×10^{-4}	6.96	3.85×10^{11}	0.3
		-0.5	1.26×10^{-4}	1.63×10^{-3}	15.04	2.37×10^{9}	
		-1.0	3.99×10^{-4}	3.01×10^{-3}	26.11	2.31×10^{9}	
	1:1.5	0	3.96×10^{-8}	9.55×10^{-4}	9.55	8.48×10^{10}	0.35
		-0.5	1.46×10^{-4}	2.20×10^{-3}	20.54	3.00×10^{9}	
		-1.0	6.02×10^{-4}	3.45×10^{-3}	28.48	2.05×10^{9}	

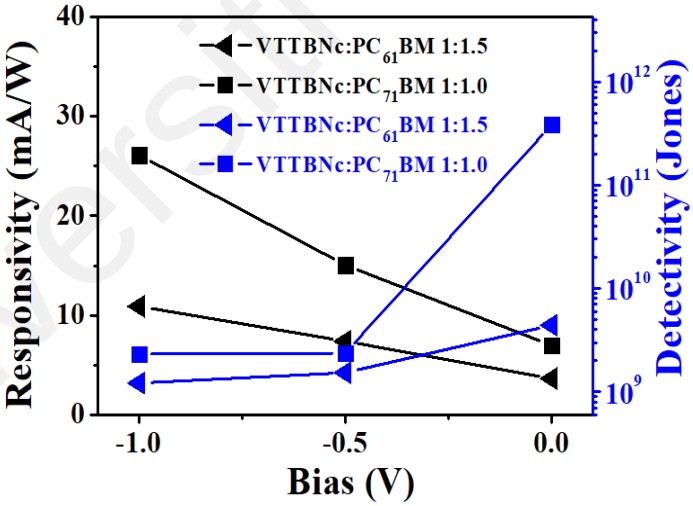

Figure 4.10: Responsivity and Detectivity of VTTBNc:$PC_{61}BM$ and VTTBNc:$PC_{71}BM$.

Figure 4.11 depicts the photo-response of VTTBNc:$PC_{61}BM$ and VTTBNc:$PC_{71}BM$ at -1 V in dark and under light illumination of 100 mW/cm^2. When the light is turned on, the response of the photocurrent increases until it reaches a steady state measured and followed by the recovery time for photocurrent fall back to the initial state when the light

is turned off. Five cycle plot has been measured under light and dark states. Table 4.5 illustrates the response and recovery time of VTTBNc:$PC_{61}BM$ and VTTBNc:$PC_{71}BM$ at -1 V for each ratio. VTTBNc:$PC_{71}BM$ of 1:1.0 ratio with highest detectivity (2.31 x 10^9 Jones), shown the measured response and recovery time of 241 ms and 310 ms, respectively. For optimized VTTBNc:$PC_{61}BM$ (1:1.5), the response and recovery time are recorded as 516 ms and 481 ms respectively. From the result, it shows that optimized VTTBNc:$PC_{71}BM$ (1:1.0) has a smaller or rapid response and recovery time compared to optimized VTTBNc:$PC_{61}BM$ (1:1.5).

It can be seen from Figure 4.11(a), there are few spikes or noise observed in VTTBNc:$PC_{61}BM$ in the dark states. For the VTTBNc:$PC_{61}BM$ of 1:0.5, there is no detection of photo-response due to the weak signal and high noise detected from the experiment. These spikes or noise might be due to the contribution of high dark current and low photocurrent generation. Meanwhile, high detectivity in VTTBNc:$PC_{71}BM$ caused the photo-response to have a stable detection in dark/light state. The main contribution of high dark current in small molecule OPD is due to the carrier injection phenomenon from electrodes that is caused by the low band gap characteristic in small molecules (Wang, Zhang, & Hu, 2020).

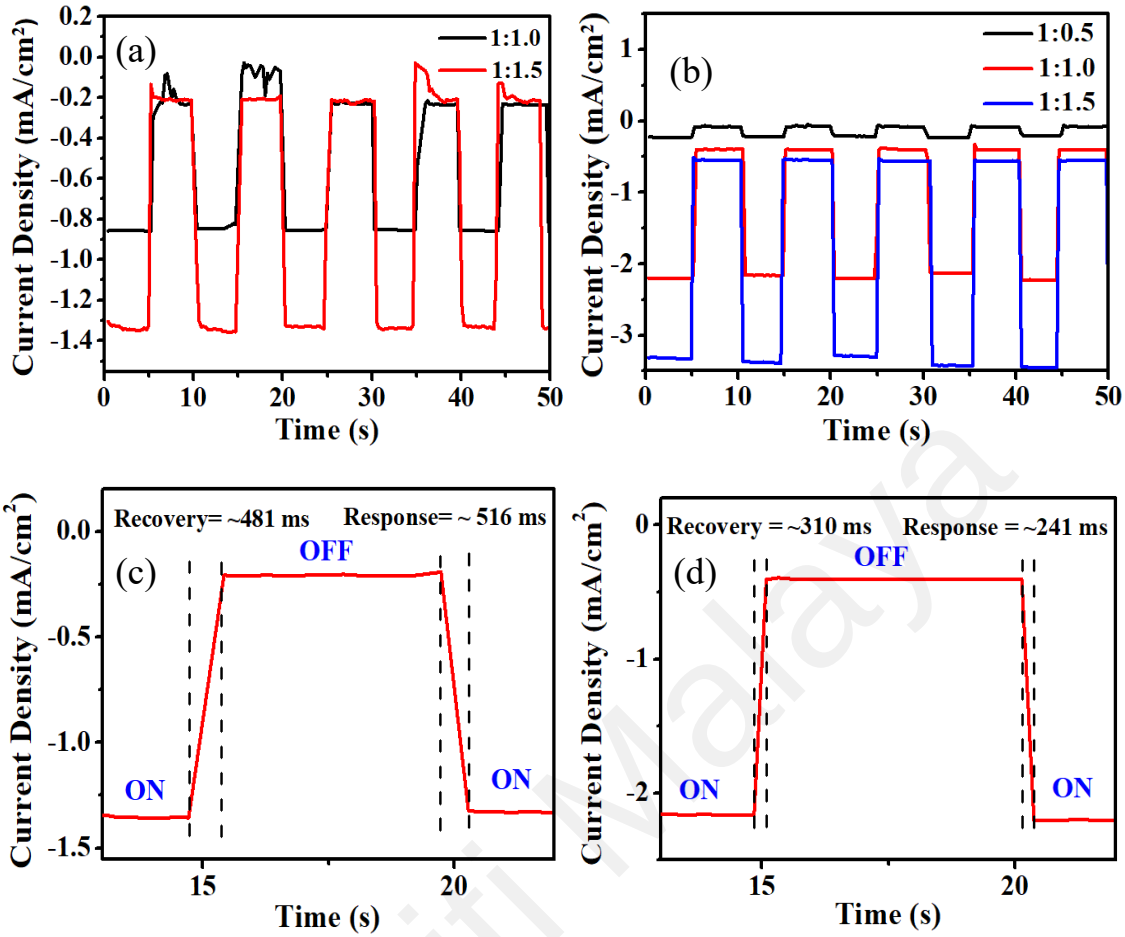

Figure 4.11: Photo-response of (a) all ratios VTTBNc:$PC_{61}BM$, (b) all ratios VTTBNc:$PC_{71}BM$, (c) optimized VTTBNc:$PC_{61}BM$ (1:1.5) (d) and optimized ratio VTTBNc:$PC_{71}BM$ (1:1.0).

Table 4.5: Response and recovery time at -1 V.

	Blend ratio	VTTBNc:$PC_{61}BM$	VTTBNc:$PC_{71}BM$
Response time (ms)	1:0.5	-	~ 242
	1:1.0	~ 518	~ 241
	1:1.5	~ 516	~ 524
Recovery time (ms)	1:0.5	-	~ 311
	1:1.0	~ 895	~ 310
	1:1.5	~ 481	~ 336

4.2.2 External Quantum Efficiency (EQE)

Figure 4.12(a) shows the external quantum efficiency (EQE) as a function of wavelength at zero bias for optimized OPD which are VTTBNc:$PC_{61}BM$ 1:1.5 and VTTBNc:$PC_{71}BM$ 1:1.0. This characterization describes the photo-conversion capability

of the OPD. It is observed that both OPD devices exhibit EQE values at 400nm, which is 2.74% for VTTBNc:$PC_{71}BM$ and 1.03% for VTTBNc:$PC_{61}BM$. The low percentage of EQE may be due to the low charge carrier generated on the photoactive layer. This hypothesis can be assumed as the EQE is defined as the ratio between the numbers of charge carriers generated to the numbers of incident photons. While in the NIR region, both devices show a reduction in EQE values compared to the visible wavelength. These results might be due to the low absorption in the NIR region of both devices as depicted in Figure 4.1 (a)&(b) that reduces charge carriers generated in the photoactive layer.

Figure 4.12(b) depicts the responsivity obtained from Photovoltaic EQE (IPCE) systems. The responsivity obtained through this method is observed in a function of wavelength at 0 V bias. From the graph, it was observed that the responsivity curve is similar to the EQE curve. This might be due to the correlation between EQE and responsivity as described in equation (3.2) & (3.3). The responsivity for both blends of VTTBNc:$PC_{71}BM$ and VTTBNc:$PC_{61}BM$ at 400 nm show the highest responsivity which are 8.85 mA/Wnm and 3.33 mA/Wnm, respectively. At the longer wavelength region, VTTBNc:$PC_{71}BM$ show the maximum responsivity of 4.54 mA/Wnm at 820 nm. While, VTTBNc:$PC_{61}BM$ show the maximum responsivity of 2.20 mA/Wnm at 745 nm. The difference in the longer wavelength position of the maximum responsivity might correspond to the number of charge carrier generation with the influence of the blend's absorption range.

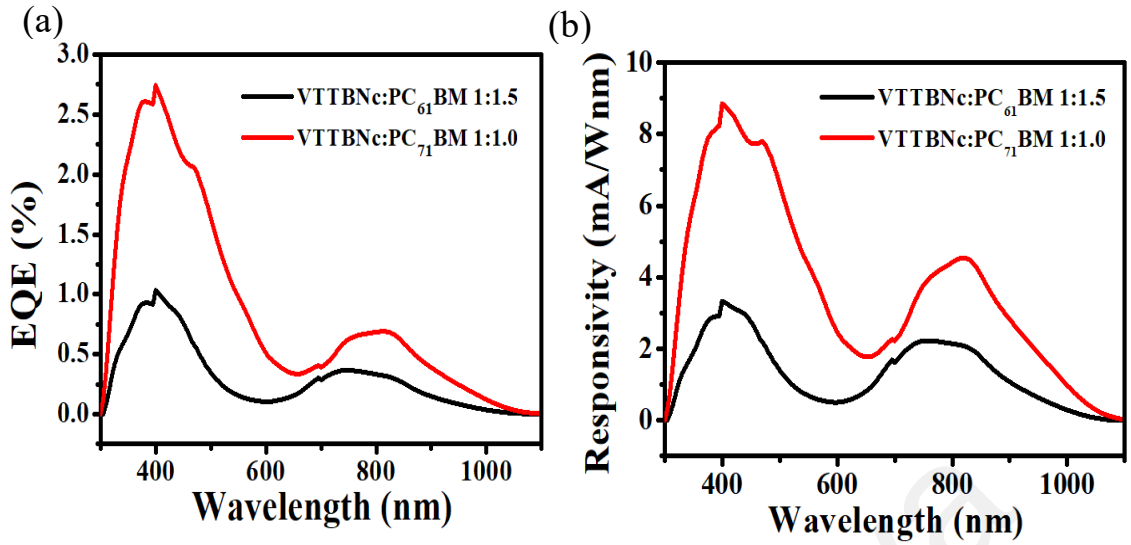

Figure 4.12: (a) External quantum efficiency (EQE) and (b) Responsivity as a function of wavelength for VTTBNc:PC_{61}BM 1:1.5 and VTTBNc:PC_{71}BM 1:1.0.

4.3 Further characterization in photoactive layer thin films

4.3.1 Photoluminescence

Further, the photoluminescence behavior of the optimized ratio for VTTBNc:PC_{61}BM (1:1.5) and VTTBNc:PC_{71}BM (1:1.0) has been observed. Figure 4.13 shows the photoluminescence (PL) spectra of VTTBNc:PC_{61}BM (1:1.5) and VTTBNc:PC_{71}BM (1:1.0) observed under excitation wavelengths of 325nm. Generally, PL measures the radiative illumination in a material. Intensity of PL spectra provides information on the recombination rate of charge carriers in order to obtain an effective charge transfer within the blended film (Motaung, Malgas, Arendse, Mavundla, & Knoesen, 2009). From the same figure, it is evident that VTTBNc:PC_{71}BM blend film has lower PL intensity than that of VTTBNc:PC_{61}BM especially in the range of 400 – 700 nm and 930 – 1150 nm. The PL spectra of VTTBNc:PC_{71}BM devices quenched around 22% compared to VTTBNc:PC_{61}BM. This quenching suggests that VTTBNc:PC_{71}BM has a more effective photo-induced charge transfer in the blended film as it demonstrates low recombination rate (Zhou et al., 2009).

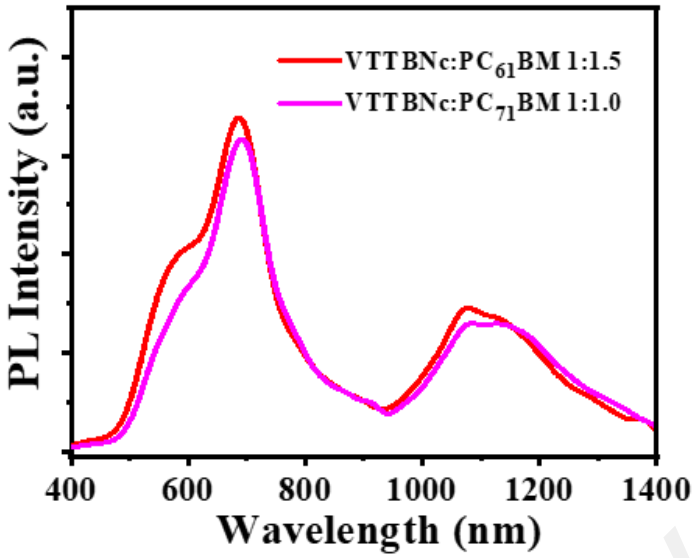

Figure 4.13: Photoluminescence spectra of VTTBNc:PC_{61}BM 1:1.5 and VTTBNc:PC_{71}BM 1:1.0.

4.3.2 Chemical structure analysis

Raman spectroscopy has been used to observe the molecular vibration mode of different blended films. In this characterization, two blend ratios which possess poor and high performance from VTTBNc:PC_{71}BM and VTTBNc:PC_{61}BM have been observed to study the causes of the best performance OPD. Figure 4.14 shows Raman spectra of VTTBNc:PC_{71}BM with ratio 1:0.5 & 1:1.0 and VTTBNc:PC_{61}BM with ratio 1:0.5 & 1:1.5. The assignments of the vibrational mode of the films have been done based on the reported literature (Makinudin, Fakir, & Supangat, 2015) as recorded in Table 4.6. It is observed that VTTBNc:PC_{71}BM exhibits a sharp peak at 1566 cm^{-1} in both ratios which refer to C=C stretching mode. Meanwhile, the peaks in VTTBNc:PC_{61}BM are dominated by lower intensity and broader peaks. The result also indicates two sharp peaks in VTTBNc:PC_{71}BM for both ratios that refer to C-H bending mode. From the literature, the sharp peak in the Raman spectra is often associated with the crystallinity and ordered structure of the film (Kotula, Snyder, & Migler, 2017; Motaung et al., 2009). Therefore, VTTBNc:PC_{71}BM films can be assumed to garner a more crystalline and ordered

structure compared to VTTBNc:$PC_{61}BM$ films. The high crystalline structure in VTTBNc:$PC_{71}BM$ supports its high OPD performance due to high charge carrier mobilities that are required for efficient charge extraction (Bartelt, Lam, Burke, Sweetnam, & McGehee, 2015; Proctor, Love, & Nguyen, 2014). On the other side, Raman intensity at 1566 cm^{-1} for VTTBNc:$PC_{71}BM$ and 1467 cm^{-1} for VTTBNc:$PC_{61}BM$ for ratio 1:0.5 is low compared to other ratios (1:1.0 and 1:1.5) due to lower content of $PC_{71}BM$ and $PC_{61}BM$ molecules.

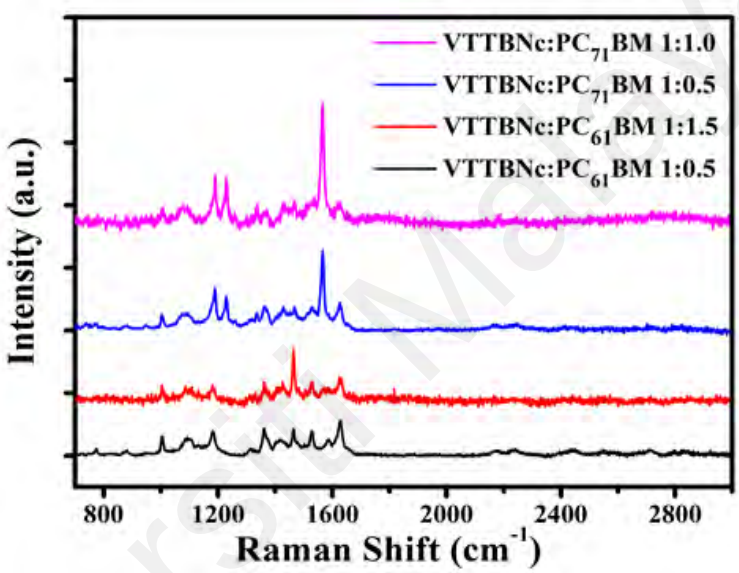

Figure 4.14: Raman spectra of VTTBNc:$PC_{61}BM$ and VTTBNc:$PC_{71}BM$.

Table 4.6: Raman shifts of VTTBNc:$PC_{71}BM$ and VTTBNc:$PC_{61}BM$.

Assignments	Raman shift (cm^{-1})			
	VTTBNc:$PC_{71}BM$		VTTBNc:$PC_{61}BM$	
	1:1.0	1:0.5	1:1.5	1:0.5
Benzene ring breath	1003	1003	1003	1003
Ring stretch	1086	1086	1092	1092
C-H bend	1190, 1227	1190, 1227	1180	1180
Pyrrole stretch	1337	1337	1316	1316
Ring stretch	1363, 1430, 1467	1363, 1430, 1467	1363, 1420, 1467	1363, 1415, 1467
Pyrrole stretch	1534	1529	1530	1530
C=C stretch	1566, 1626	1566, 1629	1582, 1629	1587, 1629

4.3.3 Morphological and Surface roughness Observations

The morphology and surface roughness of VTTBNc:$PC_{61}BM$ and VTTBNc:$PC_{71}BM$ thin film was investigated using AFM images as shown in Table 4.7. Two blend ratios which are 1:0.5 and 1:1.5 in VTTBNc:$PC_{61}BM$, while 1:0.5 and 1:1.0 in VTTBNc:$PC_{71}BM$ have been chosen based on the poor and optimized OPD. Two scan sizes with 5x5 μm and 0.5x0.5 μm have been observed to have a deep understanding of the surface morphology and roughness of the film. From the AFM images with 0.5x0.5μm scan size, the ratio with higher content of n-type exhibits high surface roughness values which are 0.546 nm for VTTBNc:$PC_{61}BM$ (1:1.5) and 0.849 nm for VTTBNc:$PC_{71}BM$ (1:1.0). Meanwhile, for a low content n-type (1:0.5) is found to be 0.284 nm for VTTBNc:$PC_{61}BM$ and 0.461 nm for VTTBNc:$PC_{71}BM$. As seen in Table 4.7 with 5x5 μm scan size, a higher content of n-type exhibits the visibility of the cluster on the surface. The presence of clusters might result in an increase of surface roughness. According to L. Benatto et al. (2020), the increase in surface roughness results in the enhancement of donor-acceptor contact area and assists the diffusion of charge carriers in the interpenetrating layer (Benatto et al., 2020). Besides, the n-types used in the blended film also affect the surface roughness values. Blended films which are VTTBNc:$PC_{71}BM$ have higher surface roughness than the VTTBNc:$PC_{61}BM$ blend film. A key difference between $PC_{61}BM$ and $PC_{71}BM$ is the axial distance for fullerene moiety. The axial distance for $PC_{61}BM$ was reported 0.70 nm and for $PC_{71}BM$ was 0.80 nm (Williams et al., 2014). The difference in axial distance in fullerene moiety might result in the difference in surface roughness values. It can be assumed that with larger axial distance in fullerene moiety contributes to the larger cluster size on the surface. Some studies also emphasize the importance of the cluster to have charge delocalization and consequently reduce recombination of the charge carrier (Kesava et al., 2014; Long et al., 2015).

Table 4.7: AFM Images.

Scan Size	5x5 µm	0.5x0.5 µm
VTTBNc:$PC_{61}BM$ (1:0.5)	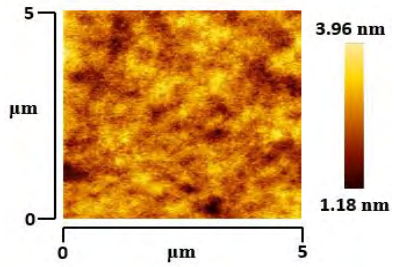	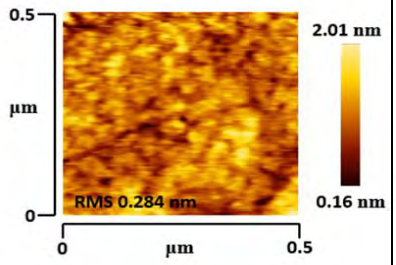
VTTBNc:$PC_{61}BM$ (1:1.5)	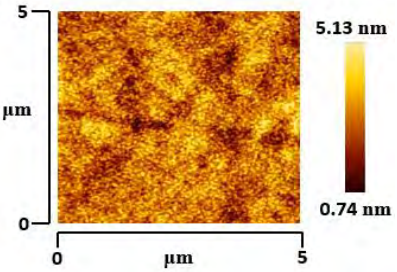	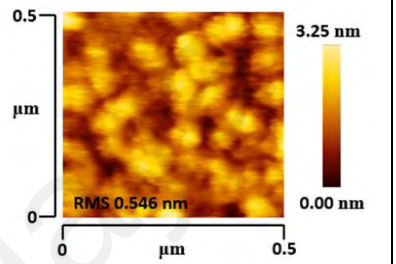
VTTBNc:$PC_{71}BM$ (1:0.5)	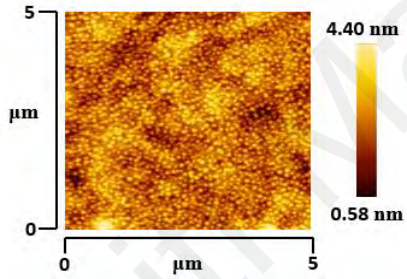	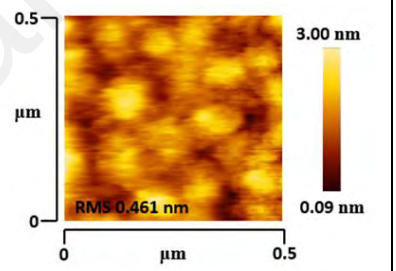
VTTBNc:$PC_{71}BM$ (1:1.0)	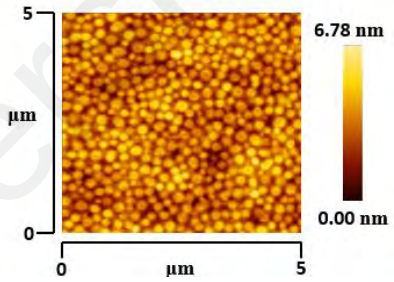	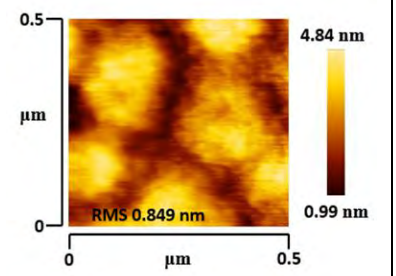

4.4 Data comparison between literature and current study.

Table 4.8 shows the findings between the literature and current study on the solution-processable naphthalocyanine-based OPD. Since 2010, there have been only two reported studies utilizing solution-processable naphthalocyanine. In 2010, Campbell investigated OPD transparency and EQE performance, and later, in 2011, Ohtani et al. only investigated the dark current, EQE, and ON/OFF ratio (Campbell, 2010; Ohtani et al., 2011). Since the detectivity and responsivity are not calculated, both studies are assumed not comprehensive because both parameters are vital in evaluating OPD's performance.

Meanwhile, the current study has conducted a comprehensive study evaluating OPD's performance and further discussed the photoactive layer's characterization. For the EQE values, Campbell obtained the highest EQE values, which is around 80%, while the current study only obtained 2.74% of EQE. Although the EQE obtained by Campbell is high, the study used high applied bias (-5 V), which will increase the charge carriers generated in the OPD and consequently increase the EQE values since EQE is the ratio of the charge carriers generated by the OPD to the number of the incident light induced. Besides that, the OPD's configuration by Campbell involved more materials in the structure that affect the fabrication to be complicated as it requires more time for the device fabrication.

Table 4.8: Findings between the literature and current study on the solution processable naphthalocyanine-based OPD.

Reference	Structure	Findings
Campbell, 2010	ITO/PEDOT:PSS/OSnNcCl$_2$/ C_{60}/BCP/CsF/Al	The study fabricated a transparent OPD with ~80% transparency and ~80% EQE in the NIR region at -5 V bias.
Ohtani et al., 2011	ITO/Cu(II)NPc:PVK:PCBM/ Al	The study found the use of conjugated polymer (PVK) to reduce dark current and n-type (PCBM) as an effective material to increase EQE values. The dark currents obtained are 10^{-4} to 10^{-6} A at -10 V bias. The lowest and highest EQE obtained are 0.24% and 9%, respectively.
Current study	ITO/PEDOT:PSS/VTTBNc: $PC_{61}BM$/Al ITO/PEDOT:PSS/VTTBNc: $PC_{71}BM$/Al	The study found the OPD utilized VTTBNc:$PC_{71}BM$ with ratio 1:1.0 has the highest detectivity of 2.31×10^9 Jones and responsivity of 26.11 mA/W with the response and recover time was found to be 241 ms and 310 ms at -1 V bias. The highest EQE obtained is 2.74% at zero bias.

CHAPTER 5: CONCLUSION AND FUTURE WORKS

5.1 Conclusion

In this dissertation, solution processable organic photodiode (OPD) devices using small molecules blend incorporate naphthalocyanine (VTTBNc) and fullerene derivatives ($PC_{61}BM$ & $PC_{71}BM$) have been successfully fabricated. VTTBNc has been utilized as an electron donor material towards fullerene derivatives as an electron acceptor. The absorption profile of VTTBNc film exhibits two broad peaks at the B-band (333 nm) and Q-band (761 nm and 810 nm) region. Meanwhile, $PC_{61}BM$ reveals a maximum absorption peak located at 335 nm and $PC_{71}BM$ has several shoulder peaks observed at 373 nm and 473 nm. Therefore, the blended films of VTTBNc:$PC_{61}BM$ and VTTBNc:$PC_{71}BM$ achieved a broader absorption spectrum (300 nm-900 nm) to the near-infrared. The study in the characterization of HOMO-LUMO levels of VTTBNc has been measured using cyclic voltammetry (CV) and ultraviolet photoelectron spectroscopy (UPS). Both methods exhibit the same value of HOMO level which indicates the accuracy in the HOMO level obtained. The LUMO level shows a slight difference in the values obtained. This uncertainty corresponds to the difference between optical and electrochemical band gap energy. The LUMO levels in the electrochemical band gap is more significant due to the similar process of the electrochemical system with charge transport in OPD. Thus, the HOMO-LUMO levels of VTTBNc were found to be as -5.14 eV and -3.74 eV which properly aligned with the energy levels in fullerene derivatives.

The optimized ratio obtained in VTTBNc:$PC_{71}BM$ and VTTBNc:$PC_{61}BM$ blend film is 1:1.0 and 1:1.5, respectively. VTTBNc:$PC_{71}BM$ with 1:1.0 ratio obtained the detectivity of 2.31×10^9 Jones and responsivity of 26.11 mA/W. While, VTTBNc:$PC_{61}BM$ obtained the detectivity of 1.21×10^9 Jones and responsivity of 10.89 mA/W at -1 V bias. Both optimized blends obtained acceptable response and recovery times in millisecond.

The response and recover time in VTTBNc:$PC_{71}BM$ (1:1.0) was found to be 241 ms and 310 ms, meanwhile in VTTBNc:$PC_{61}BM$ (1:1.5) were found to be 516 ms and 481 ms, respectively. Comprehensively, VTTBNc:$PC_{71}BM$ (1:1.0) has the highest performance among other OPD devices as a result of its considerably higher photocurrent generation compared to other study devices. Besides, morphological studies have emphasized the importance of the cluster and high surface roughness to have charge delocalization and consequently reduced recombination of the charge carrier. Therefore, the morphology of the blend by using $PC_{71}BM$ has been improved as it has higher visibility of the cluster on the surface with surface roughness increased to 62% compared to the blend using $PC_{61}BM$.

5.2 Future works

Despite the successful fabrication in solution processable OPD using VTTBNc and fullerene derivatives, there are still limitations faced that limit these OPD to be applicable to the industry used. Hence, future development needs to be implemented. Following are some propose future development that should be considered:

- The insertion of hole blocking layers such as BPhen for lowering the leakage current.
- Adding the materials with deep HOMO or shallow LUMO as the ternary material in order to minimize the holes or electrons injection from the electrode. Besides, it can enhance the photogenerated current in the photodiode.

REFERENCES

Andzelm, J., Rawlett, A. M., Orlicki, J. A., Snyder, J. F., & Baldridge, K. K. (2007). Optical properties of phthalocyanine and naphthalocyanine compounds. *Journal of Chemical Theory and Computation, 3*(3), 870-877.

Arbogast, J. W., & Foote, C. S. (1991). Photophysical properties of C_{70}. *Journal of the American Chemical Society, 113*(23), 8886-8889.

Aziz, F., Bakar, A. A., Ahmad, Z., Bawazeer, T. M., Alsenany, N., Alsoufi, M. S., & Supangat, A. (2018). Template-assisted growth of nanoporous VTTBNc films: Morphology and moisture sensitivity studies. *Materials Letters, 211*, 195-198.

Bartelt, J. A., Beiley, Z. M., Hoke, E. T., Mateker, W. R., Douglas, J. D., Collins, B. A., . . . Ade, H. (2013). The importance of fullerene percolation in the mixed regions of polymer–fullerene bulk heterojunction solar cells. *Advanced Energy Materials, 3*(3), 364-374.

Bartelt, J. A., Lam, D., Burke, T. M., Sweetnam, S. M., & McGehee, M. D. (2015). Charge-carrier mobility requirements for bulk heterojunction solar cells with high fill factor and external quantum efficiency> 90%. *Advanced Energy Materials, 5*(15), Article#1500577.

Benatto, L., Marchiori, C. F., Talka, T., Aramini, M., Yamamoto, N., Huotari, S., . . . Koehler, M. (2020). Comparing C_{60} and C_{70} as acceptor in organic solar cells: Influence of the electronic structure and aggregation size on the photovoltaic characteristics. *Thin Solid Films, 697*, Article#137827.

Blumenfeld, M. L., Steele, M. P., Ilyas, N., & Monti, O. L. (2010). Interfacial electronic structure of vanadyl naphthalocyanine on highly ordered pyrolytic graphite. *Surface Science, 604*(19-20), 1649-1657.

Campbell, I. (2010). Transparent organic photodiodes with high quantum efficiency in the near infrared. *Applied Physics Letters, 97*(3), Article#149.

Cheng, P., & Yang, Y. (2020). Narrowing the band gap: The key to high-performance organic photovoltaics. *Accounts of Chemical Research, 53*(6), 1218-1228.

Collins, S. D., Ran, N. A., Heiber, M. C., & Nguyen, T. Q. (2017). Small is powerful: Recent progress in solution-processed small molecule solar cells. *Advanced Energy Materials, 7*(10), Article#1602242.

Dalgleish, S., Reissig, L., Shuku, Y., Gourlaouen, C., Vela, S., & Awaga, K. (2018). Controlling the crystallinity and crystalline orientation of “shuttlecock” naphthalocyanine films for near-infrared optoelectronic applications. *Journal of Materials Chemistry C, 6*(8), 1959-1970.

Dhanya, I., & Menon, C. (2012). Surface morphological, structural, electrical and optical properties of annealed vanadyl tetra tert-butyl 2, 3 naphthalocyanine thin films. *Vacuum, 86*(9), 1289-1295.

Dong, H., Zhu, H., Meng, Q., Gong, X., & Hu, W. (2012). Organic photoresponse materials and devices. *Chemical Society Reviews, 41*(5), 1754-1808.

Dubinina, T., Moiseeva, E., Astvatsaturov, D., Borisova, N., Tarakanov, P., Trashin, S., . . . Tomilova, L. (2020). Novel 2-naphthyl substituted zinc naphthalocyanine: Synthesis, optical, electrochemical and spectroelectrochemical properties. *New Journal of Chemistry, 44*(19), 7849-7857.

Elgrishi, N., Rountree, K. J., McCarthy, B. D., Rountree, E. S., Eisenhart, T. T., & Dempsey, J. L. (2018). A practical beginner's guide to cyclic voltammetry. *Journal of Chemical Education, 95*(2), 197-206.

Ghani, F., Kristen, J., & Riegler, H. (2012). Solubility properties of unsubstituted metal phthalocyanines in different types of solvents. *Journal of Chemical & Engineering Data, 57*(2), 439-449.

Hori, T., Miyake, Y., Yamasaki, N., Yoshida, H., Fujii, A., Shimizu, Y., & Ozaki, M. (2010). Solution processable organic solar cell based on bulk heterojunction utilizing phthalocyanine derivative. *Applied Physics Express, 3*(10), Article#101602.

Kesava, S. V., Fei, Z., Rimshaw, A. D., Wang, C., Hexemer, A., Asbury, J. B., . . . Gomez, E. D. (2014). Domain compositions and fullerene aggregation govern charge photogeneration in polymer/fullerene solar cells. *Advanced Energy Materials, 4*(11), Article#1400116.

Kotula, A. P., Snyder, C. R., & Migler, K. B. (2017). Determining conformational order and crystallinity in polycaprolactone via raman spectroscopy. *Polymer, 117*, 1-10.

Kroto, H. W., Heath, J. R., O'Brien, S. C., Curl, R. F., & Smalley, R. E. (1985). C 60: Buckminsterfullerene. *Nature, 318*(6042), 162-163.

Kudo, K., & Moriizumi, T. (1981). Spectrum-controllable color sensors using organic dyes. *Applied Physics Letters, 39*(8), 609-611.

Lau, Y., Lan, Z., Cai, L., & Zhu, F. (2021). High-performance solution-processed large-area transparent self-powered organic near-infrared photodetectors. *Materials Today Energy, 21*, Article#100708.

Lee, C. C., Estrada, R., Li, Y. Z., Biring, S., Amin, N. R. A., Li, M. Z., . . . Wong, K. T. (2020). Vacuum-processed small molecule organic photodetectors with low dark current density and strong response to near-infrared wavelength. *Advanced Optical Materials, 8*(17), Article#2000519.

Leem, D. S., Lee, K. H., Li, N., Park, B. W., Choi, T., Ro, T., . . . Kim, S. (2021). Highly responsive and thermally reliable near-infrared organic photodiodes utilizing naphthalocyanine molecules tuned with axial ligands. *Advanced Optical Materials, 9*(4), Article#2001682.

Li, L., Huang, Y., Peng, J., Cao, Y., & Peng, X. (2014). Highly responsive organic near-infrared photodetectors based on a porphyrin small molecule. *Journal of Materials Chemistry C, 2*(8), 1372-1375.

Long, G., Li, A., Shi, R., Zhou, Y. C., Yang, X., Zuo, Y., . . . Wan, X. (2015). The evidence for fullerene aggregation in high-performance small-molecule solar cells by molecular dynamics simulation. *Advanced Electronic Materials, 1*(11), Article#1500217.

Makinudin, A. H. A., Fakir, M. S., & Supangat, A. (2015). Metal phthalocyanine: Fullerene composite nanotubes via templating method for enhanced properties. *Nanoscale Research Letters, 10*(1), Article#53.

Matthew Menke, S., Pandey, R., & Holmes, R. J. (2012). Tandem organic photodetectors with tunable, broadband response. *Applied Physics Letters, 101*(22), Article#223301.

Misra, A., Kumar, P., Srivastava, R., Dhawan, S., Kamalasanan, M., & Chandra, S. (2005). Electrochemical and optical studies of conjugated polymers for three primary colours. *Indian Journal of Pure and Applied Physics, 43*, 921-925.

Morita, S., Zakhidov, A. A., & Yoshino, K. (1992). Doping effect of buckminsterfullerene in conducting polymer: Change of absorption spectrum and quenching of luminescene. *Solid State Communications, 82*(4), 249-252.

Motaung, D. E., Malgas, G. F., Arendse, C. J., Mavundla, S. E., & Knoesen, D. (2009). Structural and photo-physical properties of spin-coated poly (3-hexylthiophene) thin films. *Materials Chemistry and Physics, 116*(1), 279-283.

Natali, D., & Caironi, M. (2016). Organic photodetectors. *Photodetectors* (pp. 195-254): Elsevier.

Nemykina, V., & Lukyanets, E. (2010). Synthesis of substituted phthalocyanines. *Arkivoc, 2010*(1), 136-208.

Ohtani, N., Nakajima, K., & Bando, K. i. (2011). Organic near-infrared photodiodes containing a wide-bandgap polymer and an n-type dopant in the active layer. *Physica Status Solidi (c), 8*(9), 2907-2910.

Orlandi, G., & Negri, F. (2002). Electronic states and transitions in C_{60} and C_{70} fullerenes. *Photochemical & Photobiological Sciences, 1*(5), 289-308.

Pandey, R., Kerner, R. A., Menke, S. M., Holst, J., Josyula, K. V., & Holmes, R. J. (2013). Tin naphthalocyanine complexes for infrared absorption in organic photovoltaic cells. *Organic Electronics, 14*(3), 804-808.

Peljo, P., & Girault, H. H. (2018). Electrochemical potential window of battery electrolytes: The HOMO–LUMO misconception. *Energy & Environmental Science, 11*(9), 2306-2309.

Proctor, C. M., Love, J. A., & Nguyen, T. Q. (2014). Mobility guidelines for high fill factor solution-processed small molecule solar cells. *Advanced Materials, 26*(34), 5957-5961.

Reissig, L., Dalgleish, S., & Awaga, K. (2018). Towards high-bandwidth organic photodetection based on pure active layer polarization. *Scientific Reports, 8*(1), 1-8.

Roslan, N. A., Abdullah, S. M., Abd Majid, W. H., & Supangat, A. (2018). Investigation of VTP: $PC_{71}BM$ organic composite as highly responsive organic photodetector. *Sensors and Actuators A: Physical, 279*, 361-366.

Sariciftci, N. S., Braun, D., Zhang, C., Srdanov, V., Heeger, A. J., Stucky, G., & Wudl, F. (1993). Semiconducting polymer-buckminsterfullerene heterojunctions: Diodes, photodiodes, and photovoltaic cells. *Applied Physics Letters, 62*(6), 585-587.

Sariciftci, N. S., Smilowitz, L., Heeger, A. J., & Wudl, F. (1992). Photoinduced electron transfer from a conducting polymer to buckminsterfullerene. *Science, 258*(5087), 1474-1476.

Scharber, M. C., & Sariciftci, N. S. (2021). Low band gap conjugated semiconducting polymers. *Advanced Materials Technologies, 6*(4), Article#2000857.

Schmidt-Mende, L., Fechtenkötter, A., Müllen, K., Moons, E., Friend, R. H., & MacKenzie, J. D. (2001). Self-organized discotic liquid crystals for high-efficiency organic photovoltaics. *Science, 293*(5532), 1119-1122.

Schulz, G. L., Urdanpilleta, M., Fitzner, R., Brier, E., Mena-Osteritz, E., Reinold, E., & Bäuerle, P. (2013). Optimization of solution-processed oligothiophene: Fullerene based organic solar cells by using solvent additives. *Beilstein Journal of Nanotechnology, 4*(1), 680-689.

Simone, G., Dyson, M. J., Meskers, S. C., Janssen, R. A., & Gelinck, G. H. (2019). Organic photodetectors and their application in large area and flexible image sensors: The role of dark current. *Advanced Functional Materials*, Article#1904205.

Su, Y.-W., Lan, S.-C., & Wei, K.-H. (2012). Organic photovoltaics. *Materials Today, 15*(12), 554-562.

Tang, C. W. (1986). Two-layer organic photovoltaic cell. *Applied Physics Letters, 48*(2), 183-185.

Tauc, J., Grigorovici, R., & Vancu, A. (1966). Optical properties and electronic structure of amorphous germanium. *Physica Status Solidi (b), 15*(2), 627-637.

Trasatti, S. (1986). The absolute electrode potential: An explanatory note. *Pure Appl. Chem, 58*(7), 955-966.

Wang, C., Zhang, X., & Hu, W. (2020). Organic photodiodes and phototransistors toward infrared detection: Materials, devices, and applications. *Chemical Society Reviews, 49*(3), 653-670.

Williams, M., Tummala, N. R., Aziz, S. G., Risko, C., & Brédas, J.-L. (2014). Influence of molecular shape on solid-state packing in disordered $PC_{61}BM$ and $PC_{71}BM$ fullerenes. *The journal of Physical Chemistry Letters, 5*(19), 3427-3433.

Yoshida, K., Oku, T., Suzuki, A., Akiyama, T., & Yamasaki, Y. (2013). Fabrication and characterization of PCBM:P3HT bulk heterojunction solar cells doped with germanium phthalocyanine or germanium naphthalocyanine. *Materials Sciences and Applications, 4*, 1-5.

Yu, G., Gao, J., Hummelen, J. C., Wudl, F., & Heeger, A. J. (1995). Polymer photovoltaic cells: Enhanced efficiencies via a network of internal donor-acceptor heterojunctions. *Science, 270*(5243), 1789-1791.

Yu, G., Pakbaz, K., & Heeger, A. (1994). Semiconducting polymer diodes: Large size, low cost photodetectors with excellent visible-ultraviolet sensitivity. *Applied Physics Letters, 64*(25), 3422-3424.

Zafar, Q., Fatima, N., Karimov, K. S., Ahmed, M. M., & Sulaiman, K. (2017). Realizing broad-bandwidth visible wavelength photodiode based on solution-processed ZnPc/PC_{71}BM dyad. *Optical Materials, 64*, 131-136.

Zheng, L., Zhu, T., Xu, W., Liu, L., Zheng, J., Gong, X., & Wudl, F. (2018). Solution-processed broadband polymer photodetectors with a spectral response of up to 2.5 μm by a low bandgap donor–acceptor conjugated copolymer. *Journal of Materials Chemistry C, 6*(14), 3634-3641.

Zhou, Y., Tvingstedt, K., Zhang, F., Du, C., Ni, W. X., Andersson, M. R., & Inganäs, O. (2009). Observation of a charge transfer state in low-bandgap polymer/fullerene blend systems by photoluminescence and electroluminescence studies. *Advanced Functional Materials, 19*(20), 3293-3299.